



AIAA 2003–5285

**MULTI-DIMENSIONAL COURANT NUMBER
INSENSITIVE CE/SE EULER SOLVERS FOR
APPLICATIONS INVOLVING HIGHLY
NONUNIFORM MESHES**

S. C. Chang

NASA Glenn Research Center, Cleveland, OH 44135

X. Y. Wang

Taitech Inc., NASA Glenn Research Center, Cleveland, OH 44135

**39th AIAA/ASME/SAE/ASEE Joint
Propulsion Conference & Exhibit
July 20–23, 2003/Huntsville, Alabama**

MULTI-DIMENSIONAL COURANT NUMBER INSENSITIVE CE/SE EULER SOLVERS FOR APPLICATIONS INVOLVING HIGHLY NONUNIFORM MESHES

S.-C. Chang* X.Y. Wang,†

*NASA Glenn Research Center, Cleveland, OH 44135

†Taitech Inc., NASA Glenn Research Center, Cleveland, OH 44135

Abstract

In a CE/SE simulation with a fixed total marching time, generally the numerical dissipation increases as the value of the CFL number decreases from 1, its maximum stability bound. As such, in a case with a large CFL number disparity (e.g., a simulation with a highly nonuniform spatial mesh and a spatially independent time step), the performance sensitivity with respect to the CFL number can lead to a solution that is highly dissipative in a region where the local CFL number $\ll 1$. In this paper, the ideas used in a recent work on one-dimensional CFL number insensitive CE/SE schemes are elaborated in a more detailed manner and also are extended to construct one-dimensional and multidimensional solvers for applications involving nonuniform spatial meshes. Also an error in a recent related paper will be described and corrected. As a by-product of the current work, a new set of wiggle-suppressing weighted-averaging formulae much more potent and flexible than those introduced earlier is also presented.

1. Introduction

The space-time conservation element and solution element (CE/SE) method is a high-resolution and genuinely multidimensional method for solving conservation laws [1–37]. Its nontraditional features include: (i) a unified treatment of space and time; (ii) the introduction of conservation elements (CEs) and solution elements (SEs) as the vehicles for enforcing space-time flux conservation; (iii) a novel time marching strategy that has a space-time staggered stencil at its core and, as such, fluxes at an interface can be evaluated without using any interpolation or extrapolation procedure (which, in turn, leads to the method’s ability to capture shocks without using Riemann solvers); (iv) the requirement that each

scheme be built from a non-dissipative core scheme and, as a result, the numerical dissipation can be controlled effectively; and (v) the mesh values of the physical dependent variables and their spatial derivatives are considered as independent marching variables to be solve for simultaneously. Note that CEs are nonoverlapping space-time subdomains introduced such that (i) the computational domain can be filled by these subdomains; and (ii) flux conservation can be enforced over each of them and also over the union of any combination of them. On the other hand, each SE is a space-time subdomain introduced such that (i) the boundary of each CE can be divided into several component parts with each of them belonging to a unique SE; and (ii) within a SE, any physical flux vector is approximated using simple smooth functions. In general, a CE does not coincide with a SE.

Without using preconditioning or other special techniques, since its inception [1] the CE/SE method has been used to obtain numerous highly accurate 1D, 2D and 3D steady and unsteady flow solutions with Mach numbers ranging from 0.0028 to 10 [28]. The flow phenomena modeled include traveling and interacting shocks, acoustic waves, shedding vortices, shock/boundary-layer interaction, detonation waves, cavitation and hydraulic jump [2–37]. In particular, the rather unique capability of the CE/SE method to resolve both strong shocks and small disturbances (e.g., acoustic waves) simultaneously [11,13,14] makes it a unique tool for attacking the problems in computational aeroacoustics (CAA). Note that the fact that the (second order) CE/SE method can solve CAA problems accurately is an exception to the commonly-held wisdom that a second-order scheme is not adequate for solving CAA problems. Also note that, while numerical dissipation is required for shock capturing, it may also result in annihilation of small disturbances. Thus a solver that can handle both strong shocks and small disturbances simultaneously must be able to overcome this difficulty.

In spite of its past successes, there is still room for improving the CE/SE method. An example is the

* Aerospace Engineer, Member AIAA
email: sin-chung.chang@grc.nasa.gov

† Research Engineer, Member AIAA
email: xiao-yen.wang@grc.nasa.gov

This paper is declared a work of the U.S. Government and is not subject to copyright protection in the United States.

fact that, in a CE/SE simulation with a fixed total marching time, generally the numerical dissipation increases as the value of the CFL number decreases from 1, its maximum stability bound. As such, in a case with a large CFL number disparity (e.g., a simulation with a highly non-uniform spatial mesh and a spatially independent time step), the performance sensitivity with respect to the CFL number can lead to a solution that is highly dissipative in a region where the local CFL number $\ll 1$.

In this paper, the ideas used in a recent work [35] on one-dimensional CFL number insensitive CE/SE schemes will be extended to construct one-dimensional and multidimensional solvers for applications involving highly nonuniform spatial meshes. Also a misconception introduced in a recent related paper [36] will be described and corrected. As a by-product of the current work, a new set of wiggle-suppressing weighted-averaging formulae much more potent and flexible than those introduced earlier [3] will also be presented. The rest of the paper is organized as follows. A review of the existing CE/SE schemes is given in Sec. 2. The new CFL number insensitive schemes are described in Secs. 3–6. Numerical results are presented in Sec. 7. Conclusions and discussions are given in Sec. 8.

2. Review of the 1D CE/SE method

For simplicity, we review the existing CE/SE schemes for the PDE

$$\frac{\partial u}{\partial t} + a \frac{\partial u}{\partial x} = 0 \quad (2.1)$$

where $a \neq 0$ is a constant. Let $x_1 = x$, and $x_2 = t$ be considered as the coordinates of a two-dimensional Euclidean space E_2 . Then, by using Gauss' divergence theorem in the space-time E_2 , it can be shown that Eq. (2.1) is the differential form of the integral conservation law

$$\oint_{S(V)} \vec{h} \cdot d\vec{s} = 0 \quad (2.2)$$

As depicted in Fig. 1, here (i) $S(V)$ is the boundary of an arbitrary *space-time* region V in E_2 , (ii) $\vec{h} = (au, u)$, and (iii) $d\vec{s} = d\sigma \vec{n}$ with $d\sigma$ and \vec{n} , respectively, being the area and the unit outward normal of a surface element on $S(V)$. Note that: (i) because $\vec{h} \cdot d\vec{s}$ is the *space-time* flux of \vec{h} leaving the region V through the surface element $d\vec{s}$, Eq. (2.2) simply states that the total *space-time* flux of \vec{h} leaving V through $S(V)$ vanishes; (ii) in E_2 , $d\sigma$ is the length of a line segment on the simple closed curve $S(V)$; and (iii) all mathematical operations can be carried out as though E_2 were an ordinary two-dimensional Euclidean space.

To proceed, let Ω denote the set of all space-time staggered mesh points in E_2 (dots in Fig. 2(a)), where $n = 0, \pm 1/2, \pm 1, \pm 3/2, \pm 2, \dots$, and, for each n , $j = n \pm 1/2, n \pm 3/2, n \pm 5/2, \dots$. Each $(j, n) \in \Omega$ is associated with a solution element, i.e., $SE(j, n)$. By definition, $SE(j, n)$ is the *interior* of the *space-time* region bounded by a dashed curve depicted in Fig. 2(b). It includes a horizontal line segment, a vertical line segment, and their immediate neighborhood.

Let $(x, t) \in SE(j, n)$. Then Eq. (2.2) will be simulated numerically assuming that $u(x, t)$ and $\vec{h}(x, t)$, respectively, are approximated by

$$u^*(x, t; j, n) \stackrel{\text{def}}{=} u_j^n + (u_x)_j^n (x - x_j) + (u_t)_j^n (t - t^n) \quad (2.3)$$

and

$$\vec{h}^*(x, t; j, n) \stackrel{\text{def}}{=} (au^*(x, t; j, n), u^*(x, t; j, n)) \quad (2.4)$$

Note that (i) u_j^n , $(u_x)_j^n$, and $(u_t)_j^n$ are constants in $SE(j, n)$, (ii) (x_j, t^n) are the coordinates of the mesh point (j, n) with $x_j = j\Delta x$ and $t^n = n\Delta t$, and (iii) Eq. (2.4) is the numerical analogue of the definition $\vec{h} = (au, u)$.

Let $u = u^*(x, t; j, n)$ satisfy Eq. (2.1) within $SE(j, n)$. Then one has $(u_t)_j^n = -a(u_x)_j^n$. As a result, Eq. (2.3) reduces to

$$u^*(x, t; j, n) = u_j^n + (u_x)_j^n [(x - x_j) - a(t - t^n)] \quad (2.5)$$

i.e., u_j^n and $(u_x)_j^n$ are the only independent marching variables associated with (j, n) .

Let E_2 be divided into nonoverlapping rectangular regions (see Fig. 2(a)). As depicted in Figs. 2(c)–2(e), (i) two such regions, i.e., $CE_-(j, n)$ and $CE_+(j, n)$, are associated with each interior mesh point $(j, n) \in \Omega$; and (ii) $CE(j, n)$ is the union of $CE_-(j, n)$ and $CE_+(j, n)$.

Given the above preliminaries, we are ready to describe the existing CE/SE solvers for Eq. (2.1).

2.1. The a scheme

Note that, among the line segments forming the boundary of $CE_-(j, n)$, \overline{AB} and \overline{AD} belong to $SE(j, n)$, while \overline{CB} and \overline{CD} belong to $SE(j-1/2, n-1/2)$. Similarly, the boundary of $CE_+(j, n)$ belongs to either $SE(j, n)$ or $SE(j+1/2, n-1/2)$. As a result, by imposing two conservation conditions at each $(j, n) \in \Omega$, i.e.,

$$\begin{aligned} \oint_{S(CE_+(j, n))} \vec{h}^* \cdot d\vec{s} &= 0, \quad \text{and} \\ \oint_{S(CE_-(j, n))} \vec{h}^* \cdot d\vec{s} &= 0, \quad (j, n) \in \Omega \end{aligned} \quad (2.6)$$

and using Eqs. (2.4) and (2.5), one can obtain two equations for the two unknowns u_j^n and $(u_x)_j^n$. In fact, let (i) $\nu \stackrel{\text{def}}{=} a\Delta t/\Delta x$, and (ii) for any $(j, n) \in \Omega$,

$$(u_{\bar{x}})_j^n \stackrel{\text{def}}{=} \frac{\Delta x}{4}(u_x)_j^n \quad (2.7)$$

then Eq.(2.6) implies that (i)

$$u_j^n = \frac{1}{2} \left\{ (1 + \nu)u_{j-1/2}^{n-1/2} + (1 - \nu)u_{j+1/2}^{n-1/2} \right. \\ \left. + (1 - \nu^2) \left[(u_{\bar{x}})_{j-1/2}^{n-1/2} - (u_{\bar{x}})_{j+1/2}^{n-1/2} \right] \right\} \quad (2.8)$$

and, assuming $|\nu| \neq 1$, (ii)

$$(u_{\bar{x}})_j^n = (u_{\bar{x}})_j^a \quad (|\nu| \neq 1) \quad (2.9)$$

with

$$(u_{\bar{x}})_j^a \stackrel{\text{def}}{=} \frac{1}{2} \left[u_{j+1/2}^{n-1/2} - u_{j-1/2}^{n-1/2} - (1 + \nu)(u_{\bar{x}})_{j+1/2}^{n-1/2} - \right. \\ \left. (1 - \nu)(u_{\bar{x}})_{j-1/2}^{n-1/2} \right] \quad (|\nu| \neq 1) \quad (2.10)$$

The a scheme, i.e., the inviscid case of the a - μ scheme [1,3,9], is formed by Eqs. (2.8) and (2.9). Note that, because

$$\frac{\partial u}{\partial \bar{x}} = \frac{\Delta x}{4} \frac{\partial u}{\partial x}$$

if $\bar{x} \stackrel{\text{def}}{=} x/(\Delta x/4)$, the *normalized* parameter $(u_{\bar{x}})_j^n$ can be interpreted as the value at (j, n) of the derivative of u with respect to the normalized coordinate \bar{x} . Also note that the superscript symbol “a” in the parameter $(u_{\bar{x}})_j^a$ is introduced to remind the reader that Eq. (2.9) is valid for the a scheme.

The review of the a scheme is concluded with the following remarks:

- (a) As shown in [3], the two amplification factors of the a scheme are identical to those of the leapfrog scheme. As a result, the a scheme is non-dissipative and it is stable if $|\nu| < 1$ (see the additional discussions given in Sec. 2.2).
- (b) Note that derivation of Eqs. (2.8) and (2.9) can be facilitated by the following observations: because $u^*(x, t; j, n)$ is linear in x and t , it can be shown that the total flux of \vec{h}^* leaving $\text{CE}_-(j, n)$ or $\text{CE}_+(j, n)$ through any of the four line segments that form its boundary is equal to the scalar product of the vector \vec{h}^* evaluated at the midpoint of the line segment and the “surface” vector (i.e., the unit outward normal multiplied by the length) of the line segment.

- (c) Because, for any $(j, n) \in \Omega$, the total flux of \vec{h}^* leaving each of $\text{CE}_-(j, n)$ and $\text{CE}_+(j, n)$ vanishes (see Eq. (2.6)), $\text{CE}_-(j, n)$ and $\text{CE}_+(j, n)$, $(j, n) \in \Omega$, will be referred to as the *conservation elements (CEs) of the a scheme*. In addition, because the surface integration over any interface separating two neighboring CEs is evaluated using the information from a single SE, obviously the flux leaving one of these CEs through the interface is the negative of that leaving another CE through the same interface. As a result, the local conservation relations Eq. (2.6) lead to a global flux conservation relation, i.e., *the total flux of \vec{h}^* leaving the boundary of any space-time region that is the union of any combination of CEs will also vanish*. In particular, because $\text{CE}(j, n)$ is the union of $\text{CE}_-(j, n)$ and $\text{CE}_+(j, n)$,

$$\oint_{S(\text{CE}(j,n))} \vec{h}^* \cdot d\vec{s} = 0, \quad (j, n) \in \Omega \quad (2.11)$$

must follow from Eq. (2.6). In fact, it can be shown that Eq. (2.11) is equivalent to Eq. (2.8).

- (d) In addition to the non-dissipative a scheme, as will be shown, there is a family of its dissipative extensions in which *only the less stringent conservation condition Eq. (2.11) is assumed* [3]. Because Eq. (2.11) is equivalent to Eq. (2.8), for each of these extensions, u_j^n is still evaluated using Eq. (2.8) while $(u_{\bar{x}})_j^n$ is evaluated using an equation different from Eq. (2.9).

2.2. The a - c scheme and the c scheme

To proceed, consider any $(j, n) \in \Omega$. Then $(j \pm 1/2, n - 1/2) \in \Omega$. Let

$$u'_{j\pm 1/2}{}^n \stackrel{\text{def}}{=} u_{j\pm 1/2}^{n-1/2} + (\Delta t/2)(u_t)_{j\pm 1/2}^{n-1/2} \quad (2.12)$$

Substituting Eq. (2.7) and the relation $(u_t)_j^n = -a(u_x)_j^n$ into Eq. (2.12) and using the definition $\nu = a\Delta t/\Delta x$, one has

$$u'_{j\pm 1/2}{}^n = (u - 2\nu u_{\bar{x}})_{j\pm 1/2}^{n-1/2} \quad (2.13)$$

Note that, to simplify notation, in the above and hereafter we adopt a convention that can be explained using the expression on the right side of Eq. (2.13) as an example, i.e.,

$$(u - 2\nu u_{\bar{x}})_{j\pm 1/2}^{n-1/2} = u_{j\pm 1/2}^{n-1/2} - 2\nu(u_{\bar{x}})_{j\pm 1/2}^{n-1/2}$$

Also note that, by definition, $(j \pm 1/2, n) \notin \Omega$ if $(j, n) \in \Omega$. Thus $u'_{j\pm 1/2}{}^n$ is associated with a mesh

point $\notin \Omega$. The reader is warned that similar situations may occur in the rest of this paper.

According to Eq. (2.12), $u'_{j\pm 1/2}$ can be interpreted as a first-order Taylor's approximation of u at $(j \pm 1/2, n)$. Thus

$$(u_{\bar{x}}^c)_j^n \stackrel{\text{def}}{=} \frac{u'_{j+1/2} - u'_{j-1/2}}{4} = \frac{\Delta x}{4} \left(\frac{u'_{j+1/2} - u'_{j-1/2}}{\Delta x} \right) \quad (2.14)$$

is a central-difference approximation of $\partial u / \partial x$ at (j, n) , normalized by the same factor $\Delta x / 4$ that appears in Eq. (2.7). Note that: (i) the superscript "c" is used to remind the reader of the central-difference nature of the term $(u_{\bar{x}}^c)_j^n$; and (ii) by using Eqs. (2.13), (2.14) and (2.8), one has

$$(u_{\bar{x}}^c)_j^n = \frac{1}{4} \left[(u - 2\nu u_{\bar{x}})_{j+1/2}^{n-1/2} - (u - 2\nu u_{\bar{x}})_{j-1/2}^{n-1/2} \right] \quad (2.15)$$

and

$$(u_{\bar{x}}^c - u_{\bar{x}}^a)_j^n = \frac{1}{2} \left[(u_{\bar{x}})_{j+1/2}^{n-1/2} + (u_{\bar{x}})_{j-1/2}^{n-1/2} \right] - \frac{1}{4} \left(u_{j+1/2}^{n-1/2} - u_{j-1/2}^{n-1/2} \right) \quad (2.16)$$

The a - ϵ scheme is formed by Eq. (2.8) and

$$(u_{\bar{x}})_j^n = (u_{\bar{x}}^a)_j^n + 2\epsilon(u_{\bar{x}}^c - u_{\bar{x}}^a)_j^n \quad (2.17)$$

where ϵ is a real number. Obviously the a - ϵ scheme reduces to the a scheme when $\epsilon = 0$. Also, for the case $\epsilon = 1/2$, Eq. (2.17) reduces to

$$(u_{\bar{x}})_j^n = (u_{\bar{x}}^c)_j^n \quad (2.18)$$

Because $(u_{\bar{x}}^c)_j^n$ represents a central-difference approximation, hereafter, to simplify its frequent references, the special a - ϵ scheme with $\epsilon = 1/2$ may be referred to simply as the c scheme.

To proceed, several key remarks about the a - ϵ scheme are presented:

- (a) At each mesh point $(j, n) \in \Omega$, Eqs. (2.8) and (2.9) are the results of two conservation conditions given in Eq. (2.6). Because Eq. (2.17) does not reduce to Eq. (2.9) except in the special case $\epsilon = 0$, at each mesh point $(j, n) \in \Omega$, generally the a - ϵ scheme satisfies only the single conservation condition Eq. (2.11) rather than the two conservation conditions Eq. (2.6). However, because $(u_{\bar{x}}^a)_j^n$ generally is present on the right side of Eq. (2.17), the a - ϵ scheme generally will still be burdened with the cost of solving two conservation conditions at each mesh point. *The exception occurs only for the special case $\epsilon = 1/2$ (i.e., the c scheme) in which*

Eq. (2.17) reduces to Eq. (2.18). As it turns out, implementation of a multidimensional Euler version of the c scheme does not require inverting any system of equations while a similar implementation involving a version of any other a - ϵ scheme ($\epsilon \neq 1/2$) generally requires inverting, per mesh point and per time step, a system of several linear equations (to be exact, a system of eight and fifteen equations, respectively, for 2D and 3D Euler equations). As such, it is much more cost effective to use a multidimensional Euler version of the c scheme than using that of any other a - ϵ scheme. Partly for this reason, extensions of the c scheme have been used extensively.

- (b) For the a - ϵ scheme, it is shown in [3] that the principal and spurious amplification factors per Δt , respectively, are $(\lambda_+)^2$ and $(\lambda_-)^2$ with

$$\lambda_{\pm}(\epsilon, \nu, \theta) \stackrel{\text{def}}{=} \epsilon \cos(\theta/2) - i\nu \sin(\theta/2) \pm \sqrt{(1-\epsilon) [(1-\epsilon)\cos^2(\theta/2) + (1-\nu^2)\sin^2(\theta/2)]} \quad (2.19)$$

Here (i) $i \stackrel{\text{def}}{=} \sqrt{-1}$, and (ii) θ , $-\pi < \theta \leq \pi$, is the phase angle variation per Δx . In addition, it is shown that (i) the necessary and sufficient conditions for the stability of the a - ϵ scheme are

$$0 \leq \epsilon \leq 1, \quad \text{and} \quad |\nu| < 1 \quad (2.20)$$

and (ii) the a - ϵ scheme becomes progressively diffusive as the value of ϵ increases from 0 to 1. Note that, unless specified otherwise, in the remainder of the paper the ranges of ϵ , ν and θ , respectively, are defined by Eq. (2.20) and $-\pi < \theta \leq \pi$.

- (c) For the plane wave solution, $u = e^{ik(x-at)}$,

the exact amplification factor per Δt

$$\stackrel{\text{def}}{=} \frac{e^{ik[x-a(t+\Delta t)]}}{e^{ik(x-at)}} = e^{-ika\Delta t} = e^{-i\nu\theta} \quad (2.21)$$

where $\theta = k\Delta x$.

- (d) According to Eq. (2.19), $[\lambda_{\pm}(0, \nu, \theta)]^2$, the amplification factors of the a scheme (which corresponds to the case $\epsilon = 0$), have the following properties:

$$|[\lambda_{\pm}(0, \nu, \theta)]^2| = 1 \quad (2.22)$$

$$\lim_{\nu \rightarrow \pm 1} [\lambda_+(0, \nu, \theta)]^2 = e^{\mp i\theta} \quad (2.23)$$

$$\lim_{\nu \rightarrow \pm 1} [\lambda_-(0, \nu, \theta)]^2 = e^{\pm i\theta} \quad (2.24)$$

and

$$[\lambda_{\pm}(0, 0, \theta)]^2 = 1 \quad (2.25)$$

On the other hand, $e^{-i\nu\theta}$, the exact amplification factor, has the following properties:

$$|e^{-i\nu\theta}| = 1 \quad (2.26)$$

$$\lim_{\nu \rightarrow \pm 1} e^{-i\nu\theta} = e^{\mp i\theta} \quad (2.27)$$

and

$$e^{-i\nu\theta} = 1 \quad \text{if} \quad \nu = 0 \quad (2.28)$$

For the a scheme, Eqs. (2.22)–(2.28) imply that: (i) the two amplification factor of the scheme, and the exact amplification factor all have the same constant absolute value ($= 1$) and, thus, the scheme is non-dissipative; (ii) in the limit of $|\nu| \rightarrow 1$ (i.e., $\nu \rightarrow 1$ or $\nu \rightarrow -1$), the principal amplification factor is identical to the exact amplification factor and, thus, the former has no dissipative or dispersive error in this limit; (iii) also in the limit of $|\nu| \rightarrow 1$, the phase angle associated with the spurious amplification factor is exactly the negative of that associated with the exact amplification factor and, thus, the spurious amplification factor has a large dispersive error in this limit except when $|\theta| \ll 1$ (i.e., when the wavelengths of the errors $\gg 1$); and (iv) when $\nu = 0$, the two amplification factors of the scheme, and the exact amplification factor are all equal to 1 and, thus, the two amplification factors of the scheme have no dissipative or dispersive error if $\nu = 0$. Because the accuracy of a scheme is essentially hinged on the behaviors of the principal amplification factor [1], according to the facts stated above, *the a scheme tends to become very accurate when $|\nu|$ approaches 1 or 0.* However, the short-wavelength errors associated with the spurious amplification factor (which could be introduced at $t = 0$ as a result of an inaccurate initial-value specification [1]) may appear in a solution as persistent (i.e., non-dissipative) numerical wiggles when $|\nu|$ approaches 1 [1,9].

- (e) According to Eq. (2.19), $[\lambda_{\pm}(1/2, \nu, \theta)]^2$, the amplification factors of the c scheme (which corresponds to the case $\epsilon = 1/2$), have the following properties:

$$\lim_{\nu \rightarrow \pm 1} [\lambda_{+}(1/2, \nu, \theta)]^2 = e^{\mp i\theta} \quad (2.29)$$

$$\lim_{\nu \rightarrow \pm 1} [\lambda_{-}(1/2, \nu, \theta)]^2 = -\sin^2(\theta/2) \quad (2.30)$$

and

$$[\lambda_{\pm}(1/2, 0, \theta)]^2 = \frac{1}{2} \left[1 \pm \cos(\theta/2) \sqrt{2 - \cos^2(\theta/2)} \right] \quad (2.31)$$

For the c scheme, Eqs. (2.27)–(2.31) imply that: (i) in the limit of $|\nu| \rightarrow 1$, the principal amplification factor is identical to the exact amplification factor and, thus, the former has no dissipative or dispersive errors in this limit; (ii) also in the limit of $|\nu| \rightarrow 1$, the spurious amplification factor has large dissipative and dispersive errors; and (iii) when $\nu = 0$, the two amplification factors of the scheme generally have large dissipative errors but no dispersive errors. According to the facts stated above, like the a scheme, the c scheme also tends to become very accurate when $|\nu|$ approaches 1. However, unlike the a scheme, the errors associated with the spurious amplification factor of the c scheme generally do die out rapidly when $|\nu|$ approaches 1. Also, in sharp contrast to the a scheme, the c scheme becomes highly dissipative when ν approaches 0.

In Sec. 3, it will be shown that new solvers of Eq. (2.1) can indeed be constructed such that they possess all the advantages but none of the disadvantages listed above. *Specifically, each of these solvers will be formed by Eq. (2.8) and a new equation in which $(u_{\bar{x}})_j^n$ is evaluated using a simple central-differencing procedure similar to that used to obtain $(u_{\bar{x}}^c)_j^n$. In addition, $(u_{\bar{x}})_j^n$ so obtained will be (i) identical to $(u_{\bar{x}}^c)_j^n$ in the limit of $|\nu| \rightarrow 1$, and (ii) identical to $(u_{\bar{x}}^a)_j^n$ when $\nu = 0$. As such, each of these new solvers (i) is comparable to the c scheme in ease of implementation; (ii) becomes the c scheme in the limit of $|\nu| \rightarrow 1$; and (iii) becomes the a scheme when $\nu = 0$.*

2.3. A special wiggle-suppressing scheme

If discontinuities are present in a numerical solution, any a - c scheme such as the c scheme is not equipped to suppress numerical wiggles that generally appear near these discontinuities. To serve as a preliminary for future development, here we shall briefly review an extension of the c scheme which was introduced as a remedy for this deficiency [3,35].

To proceed, let

$$(u_{\bar{x}-}^c)_j^n \stackrel{\text{def}}{=} \frac{1}{2} (u_j^n - u_{j-1/2}^n) = \frac{\Delta x}{4} \left(\frac{u_j^n - u_{j-1/2}^n}{\Delta x/2} \right) \quad (2.32)$$

and

$$(u_{\bar{x}+}^c)_j^n \stackrel{\text{def}}{=} \frac{1}{2}(u_{j+1/2}^n - u_j^n) = \frac{\Delta x}{4} \left(\frac{u_{j+1/2}^n - u_j^n}{\Delta x/2} \right) \quad (2.33)$$

i.e., $(u_{\bar{x}-}^c)_j^n$ and $(u_{\bar{x}+}^c)_j^n$ are two (normalized) numerical analogues of $\partial u / \partial x$ at (j, n) with one being evaluated from the left and another from the right. It can be shown that

$$(u_{\bar{x}}^c)_j^n = \frac{1}{2} (u_{\bar{x}-}^c + u_{\bar{x}+}^c)_j^n \quad (2.34)$$

i.e., $(u_{\bar{x}}^c)_j^n$ is the simple average of $(u_{\bar{x}-}^c)_j^n$ and $(u_{\bar{x}+}^c)_j^n$. As such, the c scheme can be extended by replacing $(u_{\bar{x}}^c)_j^n$ in Eq. (2.18) with an weighted average of $(u_{\bar{x}-}^c)_j^n$ and $(u_{\bar{x}+}^c)_j^n$. In other words, the resulting extension is formed by Eq. (2.8) and

$$(u_{\bar{x}})_j^n = (w_-)_j^n (u_{\bar{x}-}^c)_j^n + (w_+)_j^n (u_{\bar{x}+}^c)_j^n \quad (2.35)$$

where $(w_-)_j^n$ and $(w_+)_j^n$, the weight factors associated with $(u_{\bar{x}-}^c)_j^n$ and $(u_{\bar{x}+}^c)_j^n$ respectively, must satisfy the condition

$$(w_-)_j^n + (w_+)_j^n = 1 \quad (2.36)$$

at all $(j, n) \in \Omega$. In addition, the expression on the right side of Eq. (2.35) represents an interpolation (rather than an extrapolation) of $(u_{\bar{x}-}^c)_j^n$ and $(u_{\bar{x}+}^c)_j^n$ if and only if

$$(w_-)_j^n \geq 0 \quad \text{and} \quad (w_+)_j^n \geq 0 \quad (2.37)$$

Let x_- , x_+ , and $\alpha \geq 0$ be real variables. Let W_- and W_+ be the functions defined by: (i) $W_-(x_-, x_+; \alpha) = W_+(x_-, x_+; \alpha) = 1/2$ if $x_- = x_+ = 0$; and (ii)

$$W_-(x_-, x_+; \alpha) = \frac{|x_+|^\alpha}{|x_-|^\alpha + |x_+|^\alpha} \quad (|x_-| + |x_+| > 0) \quad (2.38a)$$

and

$$W_+(x_-, x_+; \alpha) = \frac{|x_-|^\alpha}{|x_-|^\alpha + |x_+|^\alpha} \quad (|x_-| + |x_+| > 0) \quad (2.38b)$$

if either $x_- \neq 0$ or $x_+ \neq 0$. Furthermore, let

$$(w_{\pm})_j^n = W_{\pm}((u_{\bar{x}-}^c)_j^n, (u_{\bar{x}+}^c)_j^n, \alpha) \quad (2.39)$$

Then $(w_-)_j^n$ and $(w_+)_j^n$ so defined satisfy Eqs. (2.36) and (2.37) and have the property that

$$(w_-)_j^n = (w_+)_j^n = 1/2 \quad \text{if} \quad \alpha = 0$$

$$\text{or} \quad |(u_{\bar{x}-}^c)_j^n| = |(u_{\bar{x}+}^c)_j^n| \quad (2.40)$$

Note that: (i) to avoid dividing by zero, in practice a small positive number such as 10^{-20} is added to

each of the denominators in Eqs. (2.38a,b); and (ii) the special cases of Eqs. (2.38a,b) with $\alpha = 1$ and $\alpha = 2$ are used in the slope-limiter proposed by van Leer [38], and van Albada *et al.* [39].

An extension of the c scheme is formed by Eqs. (2.8) and (2.35) with $(w_-)_j^n$ and $(w_+)_j^n$ being defined by Eq. (2.39). Let $\alpha > 0$ and $|(u_{\bar{x}-}^c)_j^n| \neq |(u_{\bar{x}+}^c)_j^n|$. Then Eqs. (2.38a,b) imply that, of $(u_{\bar{x}-}^c)_j^n$ and $(u_{\bar{x}+}^c)_j^n$, the one with smaller absolute value is associated with an weight factor $> 1/2$. This observation coupled with Eqs. (2.34)–(2.37) leads to the conclusion that, of $(u_{\bar{x}-}^c)_j^n$ and $(u_{\bar{x}+}^c)_j^n$, $(u_{\bar{x}})_j^n$ will have an algebraic value closer to the one with smaller absolute value if $(u_{\bar{x}})_j^n$ is evaluated as an weighted average of $(u_{\bar{x}-}^c)_j^n$ and $(u_{\bar{x}+}^c)_j^n$ according to Eq. (2.35). As a result, $(u_{\bar{x}})_j^n$ so evaluated has a smaller absolute value than that evaluated using Eq. (2.18). In turn, numerical wiggles or overshoots can be annihilated by the additional numerical dissipation introduced as a result of this local “flattening” of $(u_{\bar{x}})_j^n$. It has been shown numerically that the extension is stable if $|\nu| < 1$ and $\alpha \geq 0$. Moreover, as a result of Eqs. (2.18), (2.34), (2.35) and (2.40), (i) the extension reduces to the c scheme when $\alpha = 0$; and (ii) even if $\alpha > 0$, the extension behaves very much like the c scheme in any smooth solution region (where the condition $(u_{\bar{x}-}^c)_j^n = (u_{\bar{x}+}^c)_j^n$ more or less prevails) or at a solution extremum (where the condition $(u_{\bar{x}-}^c)_j^n = -(u_{\bar{x}+}^c)_j^n$ more or less prevails). As such, the wiggle-suppressing power of the extension takes effect only if $\alpha > 0$ and only in a solution region where $|(u_{\bar{x}-}^c)_j^n|$ and $|(u_{\bar{x}+}^c)_j^n|$ differ substantially.

3. The c - τ and c - τ^* schemes

In this section, the ideal solvers of Eq. (2.1) mentioned at the end of Sec. 2.2 will be constructed. As a preliminary, first we shall show that $(u_{\bar{x}}^a)_j^n$ can also be cast into a central-difference form when $\nu = 0$.

To proceed, note that by assumption $a \neq 0$. Thus $\nu = 0$ if and only if $\Delta t = 0$. Because $|\overline{EF}| = |\overline{AD}| = |\overline{CB}| = 0$ (see Fig. 2(c,d)) when $\Delta t = 0$, the two conservation conditions given in Eq. (2.6), for the case $\nu = 0$, respectively reduce to: (i) the flux leaving $\text{CE}_+(j, n)$ through the top face \overline{AF} is equal to that entering the same CE through the bottom face \overline{ED} ; and (ii) the flux leaving $\text{CE}_-(j, n)$ through the top face \overline{AB} is equal to that entering the same CE through the bottom face \overline{CD} . According to Remark (b) given at the end of Sec. 2.1, the flux leaving $\text{CE}_+(j, n)$ through the top face \overline{AF} is equal to the value of u^* at the midpoint of \overline{AF} (evaluated using the marching variables at point A) multiplied by $|\overline{AF}|$, while that entering it through the bottom face \overline{ED} is equal to the value of u^* at the midpoint

of \overline{ED} (evaluated using the marching variables at point E) multiplied by $|\overline{ED}|$. With the aid of these observations and the fact that $|\overline{AF}| = |\overline{ED}|$, the above condition (i) implies that, when $\nu = 0$, the value of u^* at the midpoint of \overline{AF} evaluated using the marching variables at point A is equal to that at the midpoint of \overline{ED} evaluated using the marching variables at point E . As such, the first conservation condition given in Eq. (2.6) is equivalent to

$$(u + u_{\bar{x}})_j^n = (u - u_{\bar{x}})_{j+1/2}^{n-1/2} \quad (\nu = 0) \quad (3.1)$$

if $\nu = 0$. Similarly, by using the above condition (ii), it can be shown that the second conservation condition given in Eq. (2.6) is equivalent to

$$(u - u_{\bar{x}})_j^n = (u + u_{\bar{x}})_{j-1/2}^{n-1/2} \quad (\nu = 0) \quad (3.2)$$

if $\nu = 0$. Because Eqs. (2.8) and (2.9) (which form the a scheme) are equivalent to Eq. (2.6) if $|\nu| \neq 1$, they must be equivalent to Eqs. (3.1) and (3.2) when $\nu = 0$. In fact, by subtracting Eq. (3.2) from Eq. (3.1), one obtains Eq. (2.9) where $(u_{\bar{x}}^a)_j^n$ is the reduced form of Eq. (2.10) for the case $\nu = 0$, i.e.,

$$(u_{\bar{x}}^a)_j^n = \frac{1}{2} \left[(u - u_{\bar{x}})_{j+1/2}^{n-1/2} - (u + u_{\bar{x}})_{j-1/2}^{n-1/2} \right] \quad (\nu = 0) \quad (3.3)$$

Similarly, by summing over Eqs. (3.1) and (3.2), one can obtain the reduced form of Eq. (2.8) for the case $\nu = 0$.

With the aid of Eq. (3.3) and the facts that: (i) $(u - u_{\bar{x}})_{j+1/2}^{n-1/2}$ and $(u + u_{\bar{x}})_{j-1/2}^{n-1/2}$, respectively, represent an approximation of u at the midpoint of \overline{ED} and that at the midpoint of \overline{CD} (see Fig. 2(c,d)); and (ii) the distance between the two midpoints referred to above is $\Delta x/2$, it becomes obvious that, for the special case $\nu = 0$, $(u_{\bar{x}}^a)_j^n$ is indeed a central-difference approximation of $\partial u / \partial x$ at $(j, n - 1/2)$ (which is identical to (j, n) when $\nu = 0$), normalized by the factor $\Delta x/4$. QED.

According to the above discussions, construction of the ideal solvers defined at the end of Sec. 2.2 is hinged on finding central-difference approximations for $(u_{\bar{x}})_j^n$ such that each approximation (i) becomes $(u_{\bar{x}}^c)_j^n$ in the limit of $|\nu| \rightarrow 1$, and (ii) reduces to the expression on the right side of Eq. (3.3) when $\nu = 0$. As a result of these observations, these new solvers can easily be constructed as the subschemes of the c - τ scheme, a new solver of Eq. (2.1) to be described immediately.

3.1. The c - τ scheme

To proceed, refer to Fig. 3. Here M_+ and M_- denote the midpoints of \overline{AF} and \overline{AB} , respectively. Also P_+ and P_- are two points on \overline{BF} that satisfy

the following two conditions: (i) P_+ is to the right (left) of M_+ if and only if P_- is to the left (right) of M_- ; and (ii) $|\overline{M_+P_+}| = |\overline{M_-P_-}|$, i.e., $\overline{M_+P_+}$ and $\overline{M_-P_-}$ have the same length. In addition, let the parameter τ be defined by: (i) $\tau \Delta x/4 = |\overline{M_+P_+}|$ if P_+ is to the right of M_+ ; and (ii) $\tau \Delta x/4 = -|\overline{M_+P_+}|$ if P_+ is to the left of M_+ . Obviously, it follows from the above definitions that (i) $\tau \Delta x/4 = |\overline{M_-P_-}|$ if P_- is to the left of M_- ; and (ii) $\tau \Delta x/4 = -|\overline{M_-P_-}|$ if P_- is to the right of M_- .

Moreover, let

$$u'(P_+) \stackrel{\text{def}}{=} [u + (\Delta t/2)u_t - (1 - \tau)(\Delta x/4)u_x]_{j+1/2}^{n-1/2} \quad (3.4)$$

$$u'(P_-) \stackrel{\text{def}}{=} [u + (\Delta t/2)u_t + (1 - \tau)(\Delta x/4)u_x]_{j-1/2}^{n-1/2} \quad (3.5)$$

By definition, $u'(P_+)$ is a first-order Taylor's approximation of u at P_+ evaluated using the marching variables at point E , while $u'(P_-)$ is a first-order Taylor's approximation of u at P_- evaluated using the marching variables at point C . Also note that, by using Eq. (2.7) and the relation $(u_t)_j^n = -a(u_x)_j^n$, Eqs. (3.4) and (3.5) can be simplified as

$$u'(P_+) = [u - (1 + 2\nu - \tau)u_{\bar{x}}]_{j+1/2}^{n-1/2} \quad (3.6)$$

and

$$u'(P_-) = [u + (1 - 2\nu - \tau)u_{\bar{x}}]_{j-1/2}^{n-1/2} \quad (3.7)$$

respectively.

At this juncture, note that P_+ and P_- generally lie outside of $\text{SE}(j + 1/2, n - 1/2)$ and $\text{SE}(j - 1/2, n - 1/2)$, respectively. Yet here, by definition, $u'(P_+)$ and $u'(P_-)$ are evaluated as though P_+ and P_- lie within $(j + 1/2, n - 1/2)$ and $(j - 1/2, n - 1/2)$, respectively. At first glance, the current practice is inconsistent with a previously established rule. However, as explained by the reasons given below, the definition of $u'(P_+)$ and $u'(P_-)$ is perfectly legitimate:

- (a) Recall that solution elements were introduced such that the boundary of a CE can be divided into several component parts with each of them belonging to a unique solution element. As such, the flux over a component part that belongs to a special solution element, say $\text{SE}(j, n)$, can be unambiguously determined in terms of the marching variables at the mesh point (j, n) . In other words, *in related to evaluation of any flux conservation condition over any CE*, Eqs. (2.3)–(2.5) can be applied only to a point $(x, t) \in \text{SE}(j, n)$.
- (b) On the other hand, $u'(P_+)$ and $u'(P_-)$ introduced here have nothing to do with flux evaluation.

tion. In fact, they will be used only in the construction of some numerical analogues of $\partial u/\partial x$ at (j, n) .

To proceed, note that: (i) A (i.e., the mesh point (j, n)) is the midpoint of $\overline{P_-P_+}$, and (ii) $|\overline{P_-P_+}| = (1 + \tau)\Delta x/2$. Thus

$$\begin{aligned} (\hat{u}_{\bar{x}})_j^n &\stackrel{\text{def}}{=} \frac{u'(P_+) - u'(P_-)}{2(1 + \tau)} \\ &= \frac{\Delta x}{4} \left(\frac{u'(P_+) - u'(P_-)}{(1 + \tau)\Delta x/2} \right) \quad (\tau \neq -1) \end{aligned} \quad (3.8)$$

represents a central-difference approximation of $\partial u/\partial x$ at the mesh point (j, n) , normalized by the factor $\Delta x/4$. Thus the new scheme formed by Eqs. (2.8) and

$$(u_{\bar{x}})_j^n = (\hat{u}_{\bar{x}})_j^n \quad (3.9)$$

represents a solver for Eq. (2.1). Because (i) $(\hat{u}_{\bar{x}})_j^n$ represents a central-difference approximation of $(u_{\bar{x}})_j^n$, and (ii) the approximation is associated with the parameter τ , hereafter the new scheme will be referred to as the c - τ scheme.

To explore the c - τ scheme, note that Eqs. (3.6)–(3.8) can be combined to yield

$$\begin{aligned} (\hat{u}_{\bar{x}})_j^n &= \frac{1}{2(1 + \tau)} \left\{ [u - (1 + 2\nu - \tau)u_{\bar{x}}]_{j+1/2}^{n-1/2} - \right. \\ &\quad \left. [u + (1 - 2\nu - \tau)u_{\bar{x}}]_{j-1/2}^{n-1/2} \right\} \quad (\tau \neq -1) \end{aligned} \quad (3.10)$$

Moreover, by using Eqs. (2.10), (2.16) and (3.10), one has

$$\begin{aligned} (\hat{u}_{\bar{x}})_j^n &= (u_{\bar{x}}^a)_j^n + \frac{2\tau}{1 + \tau} (u_{\bar{x}}^c - u_{\bar{x}}^a)_j^n \\ &\quad - \frac{\nu(1 - \tau)}{2(1 + \tau)} \left[(u_{\bar{x}})_{j+1/2}^{n-1/2} - (u_{\bar{x}})_{j-1/2}^{n-1/2} \right] \end{aligned} \quad (3.11)$$

By comparing Eq. (3.11) with (2.17), one concludes that the c - τ scheme generally is different from the a - ϵ scheme. In fact, a special case of the c - τ scheme can be turned into that of the a - ϵ scheme and vice versa if and only if either (i) $\tau = 1$ or (ii) $\nu = 0$. For the case $\tau = 1$, Eq. (3.11) implies that $(\hat{u}_{\bar{x}})_j^n = (u_{\bar{x}}^c)_j^n$. In other words, the c scheme is the special case of the c - τ scheme with $\tau = 1$, a fact that can also be deduced from the observation that the points P_+ and P_- depicted in Fig. 3, respectively, coincide with points F and B (i.e., the mesh points $(j + 1/2, n)$ and $(j - 1/2, n)$) if $\tau = 1$. On the other hand, it is seen that, when $\nu = 0$, the c - τ scheme become the a - ϵ scheme with $\epsilon = \tau/(1 + \tau)$. In fact one can further deduce that c - τ scheme reduces to the a scheme if and only if $\nu = \tau = 0$.

Furthermore, by studying the amplification matrix and the amplification factors of the c - τ scheme [40], it has been established that:

(a) The c - τ scheme is stable if

$$\tau \geq \tau_o(|\nu|), \quad \text{and} \quad |\nu| < 1 \quad (3.12)$$

where $\tau_o(s)$ ($0 \leq s < 1$) is a numerically established function. As shown in Fig. 4, $\tau_o(s)$ is a strictly increasing function of s with the following properties:

$$\tau_o(0) = 0; \quad \lim_{s \rightarrow 1^-} \tau_o(s) = 1; \quad \text{and}$$

$$0 < \tau_o(s) < s \quad \text{if} \quad 0 < s < 1 \quad (3.13)$$

(b) The c - τ scheme is also stable if $\tau > 1$ and $|\nu| = 1$. However, it is unstable if either (i) $|\nu| > 1$ or (ii) $|\nu| < 1$ and $\tau < \tau_o(|\nu|)$.

(c) For any given fixed value of $|\nu| < 1$, the c - τ scheme generally becomes more dissipative as the value of τ increases from its minimum $\tau_o(|\nu|)$. With the above preliminaries, the ideal solvers of Eq. (2.1) defined at the end of Sec. 2.2 will be constructed in Sec. 3.2.

3.2. The c - τ^* scheme

The value of τ used in the c - τ scheme generally can be chosen independent of ν . Here we consider a subset of the c - τ scheme in which τ is a function of $|\nu|$. Specifically, for each member in this subset, (i) there exists a strictly monotonically increasing smooth function $h(s)$, $0 \leq s < 1$, which has the following properties:

$$h(0) = 0; \quad \lim_{s \rightarrow 1^-} h(s) = 1; \quad \text{and}$$

$$h(s) \geq \tau_o(s) \quad \text{if} \quad 0 < s < 1 \quad (3.14)$$

and (ii)

$$\tau = h(|\nu|) \quad (|\nu| < 1) \quad (3.15)$$

Note that, using the definition of h and Eq. (3.15), one can easily infer from Fig. 3 a simple relation between the value of $|\nu|$ and the locations of P_+ and P_- , i.e., as the value of $|\nu|$ increases from 0 to 1, P_+ will move away from M_+ and edge toward the mesh point $(j + 1/2, n)$ while P_- will move away from point M_- and edge toward the mesh point $(j - 1/2, n)$. Also note that, by using Eqs. (3.13)–(3.15), one can show that: (i)

$$\tau = 0 \quad \text{if} \quad \nu = 0 \quad (3.16)$$

$$(ii) \quad \lim_{|\nu| \rightarrow 1^-} \tau = 1 \quad (3.17)$$

and (iii)

$$\tau \geq \tau_o(|\nu|) \quad (|\nu| < 1) \quad (3.18)$$

Recall that (i) $(\hat{u}_{\bar{x}})_j^n = (u_{\bar{x}}^a)_j^n$ if $\tau = \nu = 0$; and (ii) $(\hat{u}_{\bar{x}})_j^n = (u_{\bar{x}}^c)_j^n$ if $\tau = 1$. As such, Eqs. (3.16) and (3.17) imply that, for each member in the subset, (i) $(\hat{u}_{\bar{x}})_j^n = (u_{\bar{x}}^a)_j^n$ if $\nu = 0$; and (ii) $(\hat{u}_{\bar{x}})_j^n = (u_{\bar{x}}^c)_j^n$ in the limit of $|\nu| \rightarrow 1^-$. In other words, all members in the subset are ideal solvers in the domain $|\nu| < 1$. Moreover, by using Eq. (3.12) and (3.18), one can also show that these ideal solvers are also stable in the same domain.

Corresponding to infinitely many choices of h that meet all the requirements stated earlier, there are infinitely many members in the subset. One special member of this subset with

$$h(s) = s \quad (0 \leq s < 1) \quad (3.19)$$

is explored in [35]. Hereafter, the subset will be referred to simply as the $c\text{-}\tau^*$ scheme. *Also, unless specified otherwise, in the remainder of this paper Eq. (3.15) will be assumed for a given function h .*

4. Extensions of the $c\text{-}\tau^*$ scheme and related weighted averagings

To proceed, let

$$(\hat{u}_{\bar{x}-})_j^n \stackrel{\text{def}}{=} \frac{u_j^n - u'(P_-)}{1 + \tau} = \frac{\Delta x}{4} \left(\frac{u_j^n - u'(P_-)}{(1 + \tau)\Delta x/4} \right) \quad (4.1)$$

and

$$(\hat{u}_{\bar{x}+})_j^n \stackrel{\text{def}}{=} \frac{u'(P_+) - u_j^n}{1 + \tau} = \frac{\Delta x}{4} \left(\frac{u'(P_+) - u_j^n}{(1 + \tau)\Delta x/4} \right) \quad (4.2)$$

Because $|\overline{AP_-}| = |\overline{AP_+}| = (1 + \tau)\Delta x/4$ (see Fig. 3), it is easy to see that $(\hat{u}_{\bar{x}-})_j^n$ and $(\hat{u}_{\bar{x}+})_j^n$ are two normalized one-sided difference approximations of $\partial u/\partial x$ at the mesh point (j, n) with one being evaluated from the left and another from the right. Also, it follows immediately from Eqs. (3.8), (4.1) and (4.2) that

$$(\hat{u}_{\bar{x}})_j^n = \frac{1}{2} [(\hat{u}_{\bar{x}-})_j^n + (\hat{u}_{\bar{x}+})_j^n] \quad (4.3)$$

Moreover, by (i) substituting Eqs. (2.8), (3.6) and (3.7) into Eqs.(4.1) and (4.2), and (ii) using Eqs. (3.10) and (3.16), one arrives at the conclusion that

$$(\hat{u}_{\bar{x}-})_j^n = (\hat{u}_{\bar{x}+})_j^n = (\hat{u}_{\bar{x}})_j^n \quad (\nu = 0) \quad (4.4)$$

when $\nu = 0$.

With the above preliminaries, several extensions of the $c\text{-}\tau^*$ scheme will be constructed in the following subsections.

4.1. Scheme w-1

A comparison of Eqs. (4.1)–(4.3) with Eqs. (2.32)–(2.34) reveals that an obvious extension of the $c\text{-}\tau^*$ scheme can be obtained by replacing $(u_{\bar{x}-}^c)_j^n$ and $(u_{\bar{x}+}^c)_j^n$ in Eqs. (2.35) and (2.39) with $(\hat{u}_{\bar{x}-})_j^n$ and $(\hat{u}_{\bar{x}+})_j^n$, respectively. In other words, the new extension is formed by Eq. (3.8) and

$$(u_{\bar{x}})_j^n = (w_-)_j^n (\hat{u}_{\bar{x}-})_j^n + (w_+)_j^n (\hat{u}_{\bar{x}+})_j^n \quad (4.5)$$

with

$$(w_{\pm})_j^n = W_{\pm}((\hat{u}_{\bar{x}-})_j^n, (\hat{u}_{\bar{x}+})_j^n, \alpha) \quad (4.6)$$

Because the scheme is the first extension of the $c\text{-}\tau^*$ scheme in which $(u_{\bar{x}})_j^n$ is expressed as an weighted average of $(\hat{u}_{\bar{x}-})_j^n$ and $(\hat{u}_{\bar{x}+})_j^n$, for simplicity, hereafter it will be referred to as Scheme w-1. It has been shown numerically that Scheme w-1 is stable if $|\nu| < 1$ and $\alpha \geq 0$.

Note that, as a result of Eqs. (2.38a,b), (4.4) and (4.6), one concludes that, for any given $\alpha \geq 0$, $(w_-)_j^n = (w_+)_j^n = 1/2$ if $\nu = 0$. In other words, for Scheme w-1, the “weighted” average on the right side of Eq. (4.5) becomes a simple average if $\nu = 0$. According to an explanation given in the last paragraph of Sec. 2, this implies that Scheme w-1 will lose its capability to suppress wiggles or overshoots when ν becomes small. For this reason, even though the Euler version of Scheme w-1 performs much better than that of the special scheme referred to in Sec. 2.3 in its ability to resolve shocks and contact discontinuities crisply in a wide range (from 1 to less than 0.001) of the global CFL number (i.e., the maximal value of local CFL numbers), it has a serious shortcoming, i.e., wiggles or overshoots can appear near a discontinuity in a generated solution when the local CFL number there becomes extremely small. In the following, it will be shown that this weakness can be overcome by simple modifications of Eq. (4.6).

4.2. Scheme w-2

A new scheme, referred to as Scheme w-2 is formed by Eqs. (3.8) and (4.5) with $(w_{\pm})_j^n$ being given by Eq. (2.39). In other words, although $(u_{\bar{x}})_j^n$ is still constructed as an weighted average of $(\hat{u}_{\bar{x}-})_j^n$ and $(\hat{u}_{\bar{x}+})_j^n$, the associated weight factors $(w_{\pm})_j^n$ are evaluated using $(u_{\bar{x}-}^c)_j^n$ and $(u_{\bar{x}+}^c)_j^n$. Because the last two parameters, respectively, are identical to the special cases of $(\hat{u}_{\bar{x}-})_j^n$ and $(\hat{u}_{\bar{x}+})_j^n$ with $\tau \equiv 1$ (see Eqs. (2.12), (2.32), (2.33), (3.4), (3.5), (4.1), and (4.2)), their values *do not* vary with ν . As such, $(w_{\pm})_j^n \neq 1/2$ and therefore the weighted average on

the right side of Eq. (4.5) will not turn into a simple average when $\nu = 0$. In other words, Scheme w-2 is still capable of annihilating the numerical wiggles near a discontinuity even if ν becomes small. It has been shown numerically that Scheme w-2 again is stable if $|\nu| < 1$ and $\alpha \geq 0$.

Note that a possible drawback of Scheme w-2 is that the relation $|(u_{\bar{x}-}^c)_j^n| < |(u_{\bar{x}+}^c)_j^n|$ ($|(u_{\bar{x}-}^c)_j^n| > |(u_{\bar{x}+}^c)_j^n|$) does not automatically follow from $|(\hat{u}_{\bar{x}-})_j^n| < |(\hat{u}_{\bar{x}+})_j^n|$ ($|(u_{\bar{x}-})_j^n| > |(u_{\bar{x}+})_j^n|$) and vice versa. As a result, at some local mesh points, it may happen that, of $(\hat{u}_{\bar{x}-})_j^n$ and $(\hat{u}_{\bar{x}+})_j^n$, the one with smaller absolute value may not be associated with a weight factor $> 1/2$. According to a discussion given in the last paragraph of Sec. 2, this implies that there is no guarantee that, at all localities, the weighted-averaging induced numerical dissipation will be available to suppress wiggles or overshoots. Despite this possible failing, fortunately it has been demonstrated numerically that, not only are they capable of suppressing wiggles or overshoots robustly, Scheme w-2 and its Euler extensions are also highly accurate.

In the following, schemes that overcome the weakness of Scheme w-1 and also avoid the theoretically possible failing associated with Scheme w-2 will be constructed using new weighted-averaging formulae more advanced than that given in Eqs. (2.38a,b).

4.3. New weighted-averaging techniques

To pave the way, first we shall discuss a limitation of Eqs. (2.38a,b) as a generator of weight factors.

Let $x_{\pm} \neq 0$. Then, for a given $\alpha > 0$, obviously $W_- \rightarrow 1/2$ and $W_+ \rightarrow 1/2$ as $|x_+/x_-| \rightarrow 1$. As such, when $|x_+/x_-|$ is very close to 1, then both W_- and W_+ will be very close to $1/2$ *unless* $\alpha \gg 1$. As a result, in case that (i) $(\hat{u}_{\bar{x}\pm})_j^n \neq 0$, (ii) $|(\hat{u}_{\bar{x}+})_j^n|/|(\hat{u}_{\bar{x}-})_j^n|$ is very close to 1; and (iii) Eqs. (4.6) is assumed, then the only way to prevent the weighted average that appears on the right side of Eq. (4.5) from becoming almost a simple average is to increase the value of α used. However, this approach may be impracticable because numerical evaluation of a quantity such as x^α for any real number x generally is hampered by round-off errors and thus becomes highly inaccurate if the value of α becomes too large, say 100. It is the purpose of this subsection to introduce new weighted-averaging techniques that do not have the limitation discussed above.

For motivation, note that Eqs. (4.5) and (4.6) can be expressed as

$$(u_{\bar{x}})_j^n = w_1 x_1 + w_2 x_2 \quad (4.7)$$

and

$$w_1 = \frac{s_1}{s_1 + s_2} \quad \text{and} \quad w_2 = \frac{s_2}{s_1 + s_2} \quad (s_1 + s_2 > 0) \quad (4.8)$$

respectively if

$$x_1 \stackrel{\text{def}}{=} (\hat{u}_{\bar{x}-})_j^n \quad \text{and} \quad x_2 \stackrel{\text{def}}{=} (\hat{u}_{\bar{x}+})_j^n \quad (4.9)$$

$$w_1 \stackrel{\text{def}}{=} (w_-)_j^n \quad \text{and} \quad w_2 \stackrel{\text{def}}{=} (w_+)_j^n \quad (4.10)$$

$$s_1 \stackrel{\text{def}}{=} |(\hat{u}_{\bar{x}+})_j^n|^\alpha \quad \text{and} \quad s_2 \stackrel{\text{def}}{=} |(\hat{u}_{\bar{x}-})_j^n|^\alpha \quad (\alpha \geq 0) \quad (4.11)$$

Equation (4.7) represents an weighted average of only two values x_1 and x_2 . However, for the sake of generality, weighted averages of two or more values will be considered in the following development.

To proceed, let (i) N be an integer ≥ 2 , (ii) s_ℓ , $\ell = 1, 2, \dots, N$, be given positive numbers, and (iii)

$$w_\ell \stackrel{\text{def}}{=} \frac{s_\ell}{S}, \quad \ell = 1, 2, \dots, N \quad (4.12)$$

where

$$S \stackrel{\text{def}}{=} \left(\sum_{\ell=1}^N s_\ell \right) > 0 \quad (4.13)$$

(Note: to streamline the following development, here we assume that $s_\ell > 0$, $\ell = 1, 2, \dots, N$, instead of $s_\ell \geq 0$, $\ell = 1, 2, \dots, N$, as could be inferred from Eq. (4.11). However, without causing any practical harm, one can add a very small positive number, such as 10^{-20} , to each member of a set of nonnegative numbers and turn all of them into positive numbers). It follows from Eqs. (4.12) and (4.13) that

$$\sum_{\ell=1}^N w_\ell = 1, \quad \text{and} \quad 1 > w_\ell > 0, \quad \ell = 1, 2, \dots, N \quad (4.14)$$

As such,

$$W \stackrel{\text{def}}{=} \sum_{\ell=1}^N w_\ell x_\ell \quad (4.15)$$

is an ‘‘interpolated’’ weighted average of the real numbers x_ℓ . Note that, unless specified otherwise, hereafter $\ell = 1, 2, \dots, N$ is assumed.

Let

$$\delta_\ell \stackrel{\text{def}}{=} w_\ell - \frac{1}{N} \quad (4.16)$$

Then

$$w_\ell = \frac{1}{N} + \delta_\ell \quad (4.17)$$

Also, with the aid of Eq. (4.14), Eq. (4.16) implies that

$$\sum_{\ell=1}^N \delta_\ell = 0 \quad (4.18)$$

Note that W becomes the simple average of x_ℓ if all $\delta_\ell = 0$. Thus the set $\{\delta_1, \delta_2, \dots, \delta_N\}$ provides a measure of how far the weighted average is deviated from the simple average. In the following, a simple way to adjust this deviation will be introduced.

Let

$$\delta_{\min} \stackrel{\text{def}}{=} \min\{\delta_\ell\} \quad \text{and} \quad \delta_{\max} \stackrel{\text{def}}{=} \max\{\delta_\ell\} \quad (4.19)$$

Then Eq. (4.17) and the fact that $1 > w_\ell > 0$ for all ℓ imply that

$$1 > \frac{1}{N} + \delta_{\max} \quad \text{and} \quad \frac{1}{N} + \delta_{\min} > 0 \quad (4.20)$$

Let some $\delta_\ell \neq 0$ (i.e., the case with all $w_\ell = 1/N$ is excluded). Then Eq. (4.18) implies that $\delta_{\max} > 0 > \delta_{\min}$. The last inequality and Eq. (4.20) can be combined to yield

$$1 - \frac{1}{N} > \delta_{\max} > 0 > \delta_{\min} > -\frac{1}{N} \quad (\text{some } \delta_\ell \neq 0) \quad (4.21)$$

Note that an immediate result of Eq. (4.21) is

$$\sigma_{\max} \stackrel{\text{def}}{=} \min \left\{ \frac{1}{\delta_{\max}} \left(1 - \frac{1}{N}\right), -\frac{1}{N\delta_{\min}} \right\} > 1 \quad (\text{some } \delta_\ell \neq 0) \quad (4.22)$$

Given any adjustable real parameter $\sigma > 0$, let

$$\delta'_\ell \stackrel{\text{def}}{=} \sigma \delta_\ell \quad (4.23)$$

Then Eq. (4.18) implies that

$$\sum_{\ell=1}^N \delta'_\ell = 0 \quad (4.24)$$

In turn Eq. (4.24) and

$$w'_\ell \stackrel{\text{def}}{=} \frac{1}{N} + \delta'_\ell \quad (4.25)$$

imply that

$$\sum_{\ell=1}^N w'_\ell = 1 \quad (4.26)$$

As such, w'_ℓ , $\ell = 1, 2, \dots, N$, form a new set of weight factors. From Eqs. (4.23) and (4.25) one also concludes that the disparity of the weight factors (i.e., the deviation of the values of the weight factors from $1/N$) will be amplified (reduced) if $\sigma > 1$ ($\sigma < 1$).

The condition that

$$1 \geq w'_\ell \geq 0 \quad (4.27)$$

will be imposed in the current development. With the aid of Eqs. (4.23) and (4.25), and the original

assumption that $\sigma > 0$, it can be shown that, for the case that some $\delta_\ell \neq 0$, Eq. (4.27) is satisfied if and only if

$$\sigma_{\max} \geq \sigma > 0 \quad (\text{some } \delta_\ell \neq 0) \quad (4.28)$$

where σ_{\max} is defined in Eq. (4.22). On the other hand, for the special case in which all $\delta_\ell = 0$, one can conclude that $w'_\ell = 1/N$ (and thus Eq. (4.27) is satisfied) for all ℓ and all $\sigma > 0$.

Note that, according to Eq. (4.22), $\sigma_{\max} > 1$. Moreover, σ_{\max} increases as $|\delta_{\max}|$ and $|\delta_{\min}|$ decrease. In fact, $\sigma_{\max} \rightarrow +\infty$ as $\delta_{\max} \rightarrow 0^+$ and $\delta_{\min} \rightarrow 0^-$. Thus the range of the values of σ allowed becomes larger when $|\delta_{\max}|$ and $|\delta_{\min}|$ become smaller. Note that, when W defined in Eq. (4.15) almost becomes a simple average (i.e., when $|\delta_{\max}| \ll 1$ and $|\delta_{\min}| \ll 1$), the disparity of the weight factors must be amplified sharply such that the weighted average

$$W' \stackrel{\text{def}}{=} \sum_{\ell=1}^N w'_\ell x_\ell \quad (4.29)$$

will deviate substantially from the simple average. In this case, the large range of the values of σ allowed meets the need to use a large value of σ . In practice, the value of σ used is that generated using a preset formula as long as the generated value is less than or equal to σ_{\max} . For the case that the generated value is larger than σ_{\max} , $\sigma = \sigma_{\max}$ is assumed.

To be more specific, consider the $N = 2$ case in which x_ℓ and s_ℓ , $\ell = 1, 2$, are defined by Eqs. (4.9) and (4.11). It was explained earlier that, for this case, $w_1 \rightarrow 1/2$ and $w_2 \rightarrow 1/2$ as $\nu \rightarrow 0$. In other words, the weighted average $w_1 x_1 + w_2 x_2$ almost becomes a simple average when $|\nu| \ll 1$. To prevent this from happening, the weight factors w_1 and w_2 , respectively, are replaced by the new weighted factors w'_1 and w'_2 generated assuming

$$\sigma = \min \left\{ \sigma_{\max}, \frac{\sigma_o}{|\nu|} \right\} \quad (4.30)$$

where $\sigma_o > 0$ is a preset parameter in the order of 1. Note that Eq. (4.30) states that (i) $\sigma = \sigma_o/|\nu|$ if $\sigma_{\max} \geq \sigma_o/|\nu|$, and (ii) $\sigma = \sigma_{\max}$ if $\sigma_{\max} < \sigma_o/|\nu|$. As such, $\sigma \gg 1$ when $|\nu| \ll 1$.

Note that, for any $N = 2$ case, one of δ_1 and δ_2 is δ_{\max} while another is δ_{\min} . As a result, Eqs. (4.18), (4.20), and (4.22) imply that

$$0 < \delta_{\max} = -\delta_{\min} < 1/2 \quad (\text{some } \delta_\ell \neq 0) \quad (4.31)$$

and

$$\sigma_{\max} = \frac{1}{2\delta_{\max}} \quad (\text{some } \delta_\ell \neq 0) \quad (4.32)$$

Also for any case with $N = 2$, $\delta_{\max} > 0$ and $\sigma = \sigma_{\max}$, it can be shown that: (i) $w'_1 = 1$ and $w'_2 = 0$ if $\delta_1 = \delta_{\max}$, and (ii) $w'_2 = 1$ and $w'_1 = 0$ if $\delta_2 = \delta_{\max}$.

This completes the description of a new approach by which the weight factors w'_ℓ , $\ell = 1, 2, \dots, N$, are generated from the given weight factors w_ℓ , $\ell = 1, 2, \dots, N$. In the following, Another approach will be described.

To proceed, the indices of s_ℓ , $\ell = 1, 2, \dots, N$, will be reshuffled such that

$$s_N \geq s_{N-1} \geq \dots \geq s_1 > 0 \quad (4.33)$$

As such, Eqs. (4.12) and (4.13) imply that Eq. (4.14) can be replaced by a set of stronger conditions, i.e.,

$$\sum_{\ell=1}^N w_\ell = 1 \quad \text{and} \quad 1 > w_N \geq w_{N-1} \geq \dots \geq w_1 > 0 \quad (4.34)$$

Next let

$$\eta_\ell \stackrel{\text{def}}{=} \frac{s_{\ell+1}}{s_\ell} - 1, \quad \ell = 1, \dots, N-1 \quad (4.35)$$

Then (i) $\eta_\ell \geq 0$, $\ell = 1, \dots, N-1$, and (ii)

$$s_{\ell+1} = \left[\prod_{\ell'=1}^{\ell} (1 + \eta_{\ell'}) \right] s_1, \quad \ell = 1, \dots, N-1 \quad (4.36)$$

Given any adjustable real parameter $\sigma > 0$, let (i) $\tilde{s}_1 = s_1$ and

$$\tilde{s}_{\ell+1} = \left[\prod_{\ell'=1}^{\ell} (1 + \sigma \eta_{\ell'}) \right] \tilde{s}_1, \quad \ell = 1, \dots, N-1 \quad (4.37)$$

and (ii)

$$\tilde{w}_\ell \stackrel{\text{def}}{=} \frac{\tilde{s}_\ell}{\tilde{S}}, \quad \ell = 1, 2, \dots, N \quad (4.38)$$

where

$$\tilde{S} \stackrel{\text{def}}{=} \left(\sum_{\ell=1}^N \tilde{s}_\ell \right) > 0 \quad (4.39)$$

Because $\sigma > 0$ and $\eta_\ell \geq 0$, $\ell = 1, \dots, N-1$, Eq. (4.37) implies that

$$\tilde{s}_N \geq \tilde{s}_{N-1} \geq \dots \geq \tilde{s}_1 > 0 \quad (4.40)$$

Also, as a result of Eqs. (4.38)–(4.40), one has

$$\sum_{\ell=1}^N \tilde{w}_\ell = 1 \quad \text{and} \quad 1 > \tilde{w}_N \geq \tilde{w}_{N-1} \geq \dots \geq \tilde{w}_1 > 0 \quad (4.41)$$

As such, \tilde{w}_ℓ , $\ell = 1, 2, \dots, N$, form a new set of weight factors and

$$\tilde{W} \stackrel{\text{def}}{=} \sum_{\ell=1}^N \tilde{w}_\ell x_\ell \quad (4.42)$$

is an “interpolated” weighted average of the real numbers x_ℓ . Note that, for the special case that $s_N = s_{N-1} = \dots = s_1 > 0$, it is easy to see that (i) $w_\ell = \tilde{w}_\ell = 1/N$, $\ell = 1, 2, \dots, N$, and (ii) $\eta_\ell = 0$, $\ell = 1, \dots, N-1$.

Let ℓ_1 and ℓ_2 be any pair of integers with $1 \leq \ell_1 < \ell_2 \leq N$. Then Eqs. (4.12) and (4.36)–(4.38) imply that

$$\frac{w_{\ell_2}}{w_{\ell_1}} = \prod_{\ell'=\ell_1}^{\ell_2-1} (1 + \eta_{\ell'}) \quad (4.43)$$

and

$$\frac{\tilde{w}_{\ell_2}}{\tilde{w}_{\ell_1}} = \prod_{\ell'=\ell_1}^{\ell_2-1} (1 + \sigma \eta_{\ell'}) \quad (4.44)$$

Because $\sigma > 0$ and $\eta_\ell \geq 0$, $\ell = 1, \dots, N-1$, a comparison of Eqs. (4.43) and (4.44) reveals that $w_{\ell_2}/w_{\ell_1} = \tilde{w}_{\ell_2}/\tilde{w}_{\ell_1} = 1$ if $\eta_\ell = 0$ for all ℓ with $\ell_1 \leq \ell \leq (\ell_2 - 1)$. However, in case that $\eta_\ell \neq 0$ for at least one ℓ with $\ell_1 \leq \ell \leq (\ell_2 - 1)$, one has

$$\frac{\tilde{w}_{\ell_2}}{\tilde{w}_{\ell_1}} \begin{cases} > \frac{w_{\ell_2}}{w_{\ell_1}} & \text{if } \sigma > 1 \\ < \frac{w_{\ell_2}}{w_{\ell_1}} & \text{if } \sigma < 1 \\ = \frac{w_{\ell_2}}{w_{\ell_1}} & \text{if } \sigma = 1 \end{cases} \quad (4.45)$$

From the above discussions, one concludes that, except for the special case in which $s_N = s_{N-1} = \dots = s_1$, the disparity of \tilde{w}_ℓ is greater (less) than that of w_ℓ if $\sigma > 1$ ($\sigma < 1$). Note that the current approach for amplifying the weight factors has one advantage over the approach described earlier, i.e., in the current approach, there is no upper bound for the value of σ one could use. Thus, in the current approach, Eq. (4.30) is simplified as

$$\sigma = \frac{\sigma_o}{|\nu|} \quad (4.46)$$

4.4. Schemes w-3 and w-4

Consider the $N = 2$ case in which x_ℓ and s_ℓ , $\ell = 1, 2$, are defined by Eqs. (4.9) and (4.11). Let $(w'_-)_j^n$ and $(w'_+)_j^n$, respectively, be the weight factors associated with $(\hat{u}_{\bar{x}-})_j^n$ and $(\hat{u}_{\bar{x}+})_j^n$ generated using the first approach described in Sec. 4.3. Then, by definition, Scheme w-3 is formed by Eq. (2.8) and

$$(u_{\bar{x}})_j^n = (w'_-)_j^n (\hat{u}_{\bar{x}-})_j^n + (w'_+)_j^n (\hat{u}_{\bar{x}+})_j^n \quad (4.47)$$

On the other hand, let $(\tilde{w}_-)_j^n$ and $(\tilde{w}_+)_j^n$, respectively, be the weight factors associated with $(\hat{u}_{\bar{x}-})_j^n$

and $(\hat{u}_{\bar{x}+})_j^n$ generated using the second approach described in Sec. 4.3. Then, by definition, Scheme w-4 is formed by Eq. (2.8) and

$$(u_{\bar{x}})_j^n = (\tilde{w}_-)_j^n (\hat{u}_{\bar{x}-})_j^n + (\tilde{w}_+)_j^n (\hat{u}_{\bar{x}+})_j^n \quad (4.48)$$

5. Schemes for nonuniform meshes

Consider the space-time mesh $(-L \leq x \leq L$ and $t \geq 0)$ depicted in Fig. 5. Here (i) $L > 0$ is a given length, and (ii) the mesh structure in the region $-L \leq x < 0$ is the mirror image of that in the region $0 < x \leq L$.

Let the domain $0 \leq x \leq L$ on the x -coordinate line be divided into K intervals using the dividing coordinate points $\hat{x}_1, \hat{x}_2, \dots, \hat{x}_{K-1}$ where

$$0 < \hat{x}_1 < \hat{x}_2 < \dots < \hat{x}_{K-1} < L \quad (5.1)$$

Let

$$L_k \stackrel{\text{def}}{=} \hat{x}_k - \hat{x}_{k-1}, \quad k = 1, 2, \dots, K \quad (5.2)$$

with

$$\hat{x}_0 \stackrel{\text{def}}{=} 0 \quad \text{and} \quad \hat{x}_K \stackrel{\text{def}}{=} L \quad (5.3)$$

Then

$$\sum_{k=1}^K L_k = L, \quad \text{and} \quad L_k > 0, \quad k = 1, 2, \dots, K \quad (5.4)$$

In the current development, it is assumed that

$$L_k = r^{k-1} L_1, \quad k = 1, 2, \dots, K \quad (5.5)$$

where r is a parameter with

$$r > 0 \quad \text{and} \quad r \neq 1 \quad (5.6)$$

By combining Eqs. (5.4)–(5.6), one has

$$L_k = \frac{(1-r)r^{k-1}L}{1-r^K}, \quad k = 1, 2, \dots, K \quad (5.7)$$

In turn, Eqs. (5.2), (5.3), and (5.7) imply that

$$\hat{x}_k = \left(\frac{1-r^k}{1-r^K} \right) L, \quad k = 0, 1, 2, \dots, K \quad (5.8)$$

Note that, unless specified otherwise, hereafter it is assumed that $k = 1, 2, \dots, K$.

Moreover, for any k , let the interval $(\hat{x}_{k-1}, \hat{x}_k)$ be divided into M uniform sub-intervals with the dividing points $\hat{x}_{k-1}^{(1)}, \hat{x}_{k-1}^{(2)}, \dots, \hat{x}_{k-1}^{(M-1)}$ where $M > 0$ is a given integer and

$$\hat{x}_{k-1} < \hat{x}_{k-1}^{(1)} < \hat{x}_{k-1}^{(2)} < \dots < \hat{x}_{k-1}^{(M-1)} < \hat{x}_k \quad (5.9)$$

Thus

$$\hat{x}_{k-1}^{(m)} - \hat{x}_{k-1}^{(m-1)} = \ell_k, \quad m = 1, 2, \dots, M \quad (5.10)$$

where

$$\ell_k \stackrel{\text{def}}{=} \frac{L_k}{M} = \frac{(1-r)r^{k-1}}{1-r^K} \left(\frac{L}{M} \right) \quad (5.11)$$

and

$$\hat{x}_{k-1}^{(0)} \stackrel{\text{def}}{=} \hat{x}_{k-1} \quad \text{and} \quad \hat{x}_{k-1}^{(M)} \stackrel{\text{def}}{=} \hat{x}_k \quad (5.12)$$

Note that (i) the validity of the last equality sign in Eq. (5.11) follows from Eq. (5.7); and (ii) Eqs. (5.8)–(5.12) imply that

$$\hat{x}_k^{(m)} = \frac{L}{1-r^K} \left\{ 1 - \left[1 + (r-1) \frac{m}{M} \right] r^k \right\}, \quad k = 0, 1, \dots, K-1; \quad m = 0, 1, \dots, M \quad (5.13)$$

Note that $\hat{x}_K^{(0)}$ is yet to be defined. However, as a natural extension of Eq. (5.12) (i.e., let $k = K+1$ be allowed in the first part of Eq. (5.12)), it is assumed that $\hat{x}_K^{(0)} = \hat{x}_K$. According to Eq. (5.8), $\hat{x}_K = L$. Thus

$$\hat{x}_K^{(0)} \stackrel{\text{def}}{=} L \quad (5.14)$$

As will be shown, the above definition is needed in a later development. Note that, unless specified otherwise, hereafter it is assumed that $m = 1, 2, \dots, M$.

To pave the way, let

$$R(f) \stackrel{\text{def}}{=} \left\{ 0, \frac{1}{2}, 1, \frac{3}{2}, \dots, \frac{KM}{2} \right\} \quad (5.15)$$

$$D(f) \stackrel{\text{def}}{=} \{(K, 0)\} \cup \{(k, m) | k = 0, 1, \dots, K-1; m = 0, 1, \dots, M-1\} \quad (5.16)$$

By definition, (i) $R(f)$ represents a set of integers and half-integers and (ii) $D(f)$ represents a set of ordered pairs of integers. It can be shown easily that there are $(KM+1)$ elements in each of these two sets. In addition, the function f defined by

$$j = f(k, m) \stackrel{\text{def}}{=} \frac{kM+m}{2} \quad (5.17)$$

represents a one-to-one mapping between $D(f)$ and $R(f)$. For the special case $K = 3$ and $M = 4$, the values of the function f are listed in Table I. For any given $j \in R(f)$, let (i) $(k, m) = f^{-1}(j)$ where f^{-1} is the inverse of f ; and (ii)

$$x_j \stackrel{\text{def}}{=} \hat{x}_k^{(m)} \quad \text{and} \quad x_{-j} \stackrel{\text{def}}{=} -x_j \quad (5.18)$$

Hereafter, for any $j = 0, \pm 1/2, \pm 1, \dots, \pm KM/2$, the mesh line $x = x_j$ will be referred to as the j th spatial mesh line.

Next, the intersection of the j th spatial mesh line and the horizon line with $t = n\Delta t$ ($n = 0, 1/2, 1, \dots$) is considered as a mesh point (marked by a dot in Fig. 5) and denoted by (j, n) if $(j + n)$ is a half-integer. By its definition, the coordinates of (j, n) are given by

$$x = x_j \quad \text{and} \quad t = t^n \stackrel{\text{def}}{=} n\Delta t \quad (5.19)$$

In this section, the set of all (j, n) is again denoted by Ω . As shown in Fig. 6(a,b), (i) each $(j, n) \in \Omega$ is associated with two conservation element $\text{CE}_-(j, n)$ and $\text{CE}_+(j, n)$; and (ii)

$$\Delta x_j^- \stackrel{\text{def}}{=} x_j - x_{j-1/2} \quad \text{and} \quad \Delta x_j^+ \stackrel{\text{def}}{=} x_{j+1/2} - x_j \quad (5.20)$$

As a result, $\Delta x_j^- = \Delta x_{j-1/2}^+$ and $\Delta x_j^+ = \Delta x_{j+1/2}^-$. Also, as shown in Fig. 6(c),

$$\text{CE}(j, n) \stackrel{\text{def}}{=} \text{CE}_-(j, n) \cup \text{CE}_+(j, n) \quad (5.21)$$

and

$$\Delta x_j \stackrel{\text{def}}{=} x_{j+1/2} - x_{j-1/2} = \Delta x_j^- + \Delta x_j^+ \quad (5.22)$$

Hereafter, the midpoint of the top face of $\text{CE}(j, n)$ is referred to as the solution point (marked by a cross in Fig. 6(c)) associated with the mesh point (j, n) and is denoted by $(j, n)'$. As shown in Fig. 5, a solution point may or may not coincides with a mesh point. Also, as depicted in Fig. 6(d), each $(j, n)'$ is associated with a solution element $\text{SE}(j, n)$. Note that, by its definition, the coordinates of $(j, n)'$ are given by

$$x = x_j' \stackrel{\text{def}}{=} \frac{1}{2}(x_{j-1/2} + x_{j+1/2}) \quad \text{and} \quad t = t^n \quad (5.23)$$

In addition, the midpoint of the line segment joining (j, n) and $(j + 1/2, n)$, and that of line segment joining (j, n) and $(j - 1/2, n)$ are marked by circles (see Fig. 6(c)) and, respectively, denoted by $(j, n)^+$ and $(j, n)^-$. Note that the line segment joining (j, n) and $(j + 1/2, n)$, and that joining (j, n) and $(j - 1/2, n)$ are the top faces of $\text{CE}_+(j, n)$ and $\text{CE}_-(j, n)$, respectively. As such, $(j, n)^+$ and $(j, n)^-$ are the current counterparts of points M_+ and M_- depicted in Fig. 3. By their definitions, the coordinates of $(j, n)^+$ and $(j, n)^-$ are given by

$$x = x_j^+ \stackrel{\text{def}}{=} \frac{1}{2}(x_j + x_{j+1/2}) \quad \text{and} \quad t = t^n \quad (5.24)$$

and

$$x = x_j^- \stackrel{\text{def}}{=} \frac{1}{2}(x_j + x_{j-1/2}) \quad \text{and} \quad t = t^n \quad (5.25)$$

respectively.

Furthermore, by using Eqs. (5.20), (5.23) and (5.24), it can be shown that

$$x_j^- - x_{j-1/2}' = \frac{1}{2}\Delta x_{j-1/2}^- > 0 \quad (5.26)$$

$$x_{j+1/2}' - x_j^+ = \frac{1}{2}\Delta x_{j+1/2}^+ > 0 \quad (5.27)$$

$$x_j' - x_j^- = \frac{1}{2}\Delta x_j^+ > 0 \quad (5.28)$$

$$x_j^+ - x_j' = \frac{1}{2}\Delta x_j^- > 0 \quad (5.29)$$

$$x_j - x_{j-1/2}' = \frac{1}{2}\Delta x_{j-1/2}^- > 0 \quad (5.30)$$

$$x_{j+1/2}' - x_j = \frac{1}{2}\Delta x_{j+1/2}^+ > 0 \quad (5.31)$$

$$x_{j+1/2}' - x_j' = \frac{1}{2} \left[\Delta x_j^- + \Delta x_{j+1/2}^+ \right] > 0 \quad (5.32)$$

The relations Eqs. (5.20), and (5.22)–(5.32) are clearly illustrated in Fig. 7.

The current counterparts of points P_+ and P_- depicted in Fig. 3 are points P_{+j} and P_{-j} depicted in Fig. 7. By definition, the coordinates of points P_{+j} and P_{-j} , respectively, are given by

$$x = x(P_{+j}) \quad \text{and} \quad t = t^n \quad (5.33)$$

and

$$x = x(P_{-j}) \quad \text{and} \quad t = t^n \quad (5.34)$$

with

$$\begin{aligned} x(P_{+j}) &\stackrel{\text{def}}{=} x_j^+ + \tau_j(x_{j+1/2}' - x_j^+) = x_j^+ + \frac{\tau_j}{2}\Delta x_{j+1/2}^+ \\ &= x_{j+1/2}' - \frac{1 - \tau_j}{2}\Delta x_{j+1/2}^+ \end{aligned} \quad (5.35)$$

$$\begin{aligned} x(P_{-j}) &\stackrel{\text{def}}{=} x_j^- + \tau_j(x_{j-1/2}' - x_j^-) = x_j^- - \frac{\tau_j}{2}\Delta x_{j-1/2}^- \\ &= x_{j-1/2}' + \frac{1 - \tau_j}{2}\Delta x_{j-1/2}^- \end{aligned} \quad (5.36)$$

Here note that: (i) τ_j , with the range

$$0 \leq \tau_j \leq 1 \quad (5.37)$$

is a parameter to be defined later; and (ii) as the value of τ_j increases from 0 to 1, P_{+j} will move away from $(j, n)^+$ and edge toward the solution point $(j + 1/2, n)'$ while P_{-j} will move away from $(j, n)^-$ and edge toward the solution point $(j - 1/2, n)'$.

This completes the specification of key geometric parameters. Next note that, the current counterpart to Eq. (2.3) is

$$u^*(x, t; j, n) \stackrel{\text{def}}{=} u_j^n + (u_x)_j^n(x - x_j') + (u_t)_j^n(t - t^n) \quad (5.38)$$

i.e., u_j^n is the value of u^* at the solution point $(j, n)'$. Because $(u_t)_j^n = -a(u_x)_j^n$ is also assumed here, the current counterpart to Eq. (2.5) is

$$u^*(x, t; j, n) = u_j^n + (u_x)_j^n [(x - x_j') - a(t - t^n)] \quad (5.39)$$

Obviously, Eq. (2.4) is valid even for the current case. By imposing Eq. (2.11), and using Eqs. (2.4) and (5.39), one can obtain the current counterpart to Eq. (2.8), i.e.,

$$\begin{aligned} u_j^n &= \frac{\Delta x_j^+}{\Delta x_j} \left[u_{j+1/2}^{n-1/2} + (u_x)_{j+1/2}^{n-1/2} (x_j^+ - x'_{j+1/2}) \right] \\ &+ \frac{\Delta x_j^-}{\Delta x_j} \left[u_{j-1/2}^{n-1/2} + (u_x)_{j-1/2}^{n-1/2} (x_j^- - x'_{j-1/2}) \right] \\ &- \frac{a\Delta t}{2\Delta x_j} \left[u_{j+1/2}^{n-1/2} + (u_x)_{j+1/2}^{n-1/2} (x_{j+1/2} - x'_{j+1/2}) \right. \\ &\quad \left. - \frac{a\Delta t}{4} (u_x)_{j+1/2}^{n-1/2} \right] \\ &+ \frac{a\Delta t}{2\Delta x_j} \left[u_{j-1/2}^{n-1/2} + (u_x)_{j-1/2}^{n-1/2} (x_{j-1/2} - x'_{j-1/2}) \right. \\ &\quad \left. - \frac{a\Delta t}{4} (u_x)_{j-1/2}^{n-1/2} \right] \end{aligned} \quad (5.40)$$

Note that, normalized numerical analogues of $\partial u / \partial x$ are not used in this section.

Next, let

$$u'(P_{+j}) \stackrel{\text{def}}{=} u^*(x(P_{+j}), t^n; j + 1/2, n - 1/2) \quad (5.41)$$

and

$$u'(P_{-j}) \stackrel{\text{def}}{=} u^*(x(P_{-j}), t^n; j - 1/2, n - 1/2) \quad (5.42)$$

By using Eqs. (5.35), (5.36), and (5.39), Eqs. (5.41) and (5.42) imply

$$\begin{aligned} u'(P_{+j}) &= u_{j+1/2}^{n-1/2} + \\ &\left[(1 - \tau_j)(x_j^+ - x'_{j+1/2}) - (a\Delta t/2) \right] (u_x)_{j+1/2}^{n-1/2} \end{aligned} \quad (5.43)$$

and

$$\begin{aligned} u'(P_{-j}) &= u_{j-1/2}^{n-1/2} + \\ &\left[(1 - \tau_j)(x_j^- - x'_{j-1/2}) - (a\Delta t/2) \right] (u_x)_{j-1/2}^{n-1/2} \end{aligned} \quad (5.44)$$

respectively. Eqs. (5.43) and (5.44) are the current counterparts to Eqs. (3.6) and (3.7), respectively.

Next, the current counterparts to Eqs. (4.1) and (4.2) are

$$(\hat{u}_{x-})_j^n \stackrel{\text{def}}{=} \frac{u_j^n - u'(P_{-j})}{x_j' - x(P_{-j})} \quad (5.45)$$

and

$$(\hat{u}_{x+})_j^n \stackrel{\text{def}}{=} \frac{u'(P_{+j}) - u_j^n}{x(P_{+j}) - x_j'} \quad (5.46)$$

respectively. Note that it can be shown easily that the denominators in Eqs. (5.45) and (5.46) are positive always. By using one of many approaches described earlier, one can generate $(w_-)_j^n$ and $(w_+)_j^n$, the weight factors associated with $(\hat{u}_{x-})_j^n$ and $(\hat{u}_{x+})_j^n$. Given $(w_-)_j^n$ and $(w_+)_j^n$, a solver can be formed by Eq. (5.40) and

$$(u_x)_j^n = (w_-)_j^n (\hat{u}_{x-})_j^n + (w_+)_j^n (\hat{u}_{x+})_j^n \quad (5.47)$$

To complete the description of the current solvers, note that, among many possible choices, one may assume that

$$\tau_j = |a\Delta t / e_j|, \quad j = 0, \pm 1/2, \pm 1, \pm 3/2, \dots, \pm(KM-1)/2 \quad (5.48)$$

where e_j are positive constants defined by: (i)

$$e_j \stackrel{\text{def}}{=} \min\{(x_j' - x'_{j-1}), (x'_{j+1} - x_j')\} \quad (5.49a)$$

if $j = 0, \pm 1/2, \pm 1, \dots, \pm(KM-2)/2$; (ii)

$$e_j \stackrel{\text{def}}{=} \min\{2(x_j' - x'_{j-1/2}), (x'_{j+1} - x_j')\} \quad (5.49b)$$

if $j = -(KM-1)/2$; and (iii)

$$e_j \stackrel{\text{def}}{=} \min\{2(x'_{j+1/2} - x_j'), (x_j' - x'_{j-1})\} \quad (5.49c)$$

if $j = (KM-1)/2$

Note that τ_j given in Eq. (5.48) can be interpreted as the CFL number at $(j, n)'$. In other words, Eq. (5.48) is the current counterpart of a special case of Eq. (3.15) in which $h(s) = s$. Also Note that, because $x_{(KM+1)/2}$ and $x_{-(KM+1)/2}$ are undefined, $x'_{\pm KM/2}$ cannot be defined using Eq. (5.23). However, according to Eq. (5.49), $x'_{\pm KM/2}$ are needed in the definitions of $e_{\pm(KM-1)/2}$. As such, here we assume that

$$x'_{\pm KM/2} = x_{\pm KM/2} \quad (5.50)$$

Also, to satisfy Eq. (5.37) for all values of j , Δt is subjected to the condition that

$$\Delta t \leq \frac{\min\{e_j\}}{|a|} \quad (5.51)$$

We conclude this section with a discussion of Eq. (5.11) for the special case in which $r^K \gg 1$. For the case $r^K \gg 1$, Eq. (5.11) implies that

$$\ell_K = \frac{(1-r)r^{K-1}}{1-r^K} \cdot \frac{L}{M} \approx \frac{(1-r)r^{K-1}}{-r^K} \cdot \frac{L}{M}$$

$$= \frac{r-1}{r} \cdot \frac{L}{M} \quad (r^K \gg 1) \quad (5.52)$$

In turn, Eq. (5.52) implies that

$$r \approx \frac{1}{1 - M(\ell_K/L)} \quad (r^K \gg 1) \quad (5.53)$$

Finally, by combining Eqs. (5.7) and (5.53), one has

$$R \stackrel{\text{def}}{=} \frac{L_K}{L_1} = r^{K-1} \approx \left(\frac{1}{1 - M(\ell_K/L)} \right)^{K-1} \quad (r^K \gg 1) \quad (5.54)$$

Thus, for the case $r^K \gg 1$, r and therefore R can be easily evaluated in terms of M and the ratio ℓ_K/L without using an iterative procedure, as would be expected if Eq. (5.11) is used directly.

6. Two-dimensional extensions using triangular meshes

Several 2D CE/SE schemes using triangular meshes were described in [7,8]. These 2D schemes also can be easily modified to become CFL number insensitive schemes. A sketch explaining how this can be done is given here.

Consider Fig. 8. Here, a triangle $\triangle ABC$ is surrounded by three neighboring triangles $\triangle ADB$, $\triangle BEC$ and $\triangle CFA$. The centroids of $\triangle ABC$, $\triangle ADB$, $\triangle BEC$, and $\triangle CFA$ are denoted by G , G_1 , G_2 , and G_3 , respectively.

Let the plane shown in Fig. 8 be a x - y plane at the time level $t = t^n$, $n = 0, 1/2, 1, \dots$. Then G can be considered as a mesh point at $t = t^n$. As shown in [7,8], the three conservation elements associated with G are three quadrilateral space-time cylinders sandwiched between the time level at $t = t^n$ and that at $t = t^{n-1/2}$ with their top faces being GAG_1B , GBG_2C , and GCG_3A , respectively. The centroids of the above three top faces are denoted by M_1 , M_2 and M_3 , respectively. M_1 , M_2 , and M_3 , are the current counterparts to points $(j, n)^+$ and $(j, n)^-$ depicted in Fig. 7 (or points M_+ and M_- depicted in Fig. 3).

Furthermore, let the solution point associated with point G be the centroid of the hexagon $AG_1BG_2CG_3$ (which is the union of the three top faces referred to in the last paragraph) and denoted by G' (not shown in Fig. 8). In general, G' does not coincide with G . Also G and G' are current counterparts to (j, n) and $(j, n)'$ depicted in Figs. 6 and 7. The solution points associated with G_1 , G_2 , and G_3 can be defined similarly and denoted by G'_1 , G'_2 , and G'_3 , respectively. The projections of G'_1 , G'_2 , and G'_3 at the time level $t = t^{n-1/2}$ are the current counterparts to $(j + 1/2, n - 1/2)'$ and $(j - 1/2, n - 1/2)'$ depicted in Fig. 7.

In addition, note that points P_1 , P_2 , and P_3 depicted in Fig. 8 are the current counterparts to

points P_{+j} and P_{-j} depicted in Fig. 7. By definition, they lie on the line segments $\overline{M_1G'_1}$, $\overline{M_2G'_2}$, and $\overline{M_3G'_3}$, respectively. (Note: in Fig. 8, G'_1 , G'_2 , and G'_3 happen to coincide with G_1 , G_2 and G_3 , respectively.) It is also assumed that

$$\frac{|M_\ell P_\ell|}{|M_\ell G'_\ell|} = \tau(G'), \quad \ell = 1, 2, 3 \quad (6.1)$$

where $\tau(G')$ is the current counterpart to τ_j (see Eq. (5.48)) and is subjected to the condition

$$0 \leq \tau(G) \leq 1 \quad (6.2)$$

Finally note that, *points M_1 , M_2 , and M_3 were incorrectly defined in [36] as the midpoints of the line segments $\overline{G'G'_1}$, $\overline{G'G'_2}$, and $\overline{G'G'_3}$, respectively.*

7. Numerical results

The solvers described in this paper, in a straightforward manner described in [3,7,8], have been extended to become their Euler versions. Accuracy of of these Euler solvers will be assessed here.

7.1 Sod's Shock-tube problem

First, accuracy of the 1D uniform-mesh Euler versions of the special scheme described in Sec. 2.3 and Scheme w-4 are evaluated using Sod's shock tube problem [41]. The results are shown in Figs. 9 and 10 with the understanding that the "old" solutions are generated using the special scheme with $\alpha = 1$ (see Eq. (2.39)) while the new solutions are generated using Scheme w-4 with $\alpha = 1$ and $\sigma_o = 0.5$ (see Eqs. (4.11), and (4.46)). Here the spatial domain is defined by $-0.505 \leq x \leq 0.505$ with $\Delta x = 0.01$. The numerical results at $t = 0.2$, including density (ρ), velocity (u) and pressure (p), are presented for two different sizes of time step, i.e., (i) $\Delta t = 4 \times 10^{-3}$ (Fig. 9); and (ii) $\Delta t = 4 \times 10^{-6}$ (Fig. 10). The values of the global CFL number for these two cases approximately are 0.88 and 0.00088, respectively. Because each marching step advances a time period $\Delta t/2$, it requires 100 and 100,000 marching steps for cases (i) and (ii), respectively, to advance to $t = 0.2$.

From the results shown, it is clear that the old CE/SE solutions are highly dissipative when the value of global CFL number $\ll 1$. In sharp contrast, the new solutions are still quite accurate even when CFL number < 0.001 . The advantage of Scheme w-4 over the scheme described in Sec. 2.3 is overwhelming.

Next, accuracy of the 1D nonuniform-mesh Euler versions of Scheme w-3 ($\alpha = 2$ and $\sigma_o = 1$) are also evaluated using Sod's shock tube problem. The results obtained using three different nonuniform meshes are shown in Figs. 11–13. Using the

geometric parameters defined in Sec. 5, the three meshes, respectively, are defined by (i) $L = 0.5$, $r = 1/0.96$, $M = 4$, and $K = 170$; (ii) $L = 0.5$, $r = 2$, $M = 50$, and $K = 11$; and (iii) $L = 0.5$, $r = 4$, $M = 75$, and $K = 6$. By using Eqs. (5.53) and (5.54), it is easy to shown that (i) $\ell_K/L = 0.01$ for all three cases, and (ii) $R \approx 1000$ for case (i) and $R = 1024$ for cases (ii) and (iii). The numerical results ($t = 0.2$) are generated after 100,000 marching steps assuming $\Delta t = 4 \times 10^{-6}$.

Because $R = \ell_K/\ell_1 \approx 1000$, the variation in mesh intervals is very large for all three cases. As a result, the disparity in CFL numbers is also very large—they vary from 0.88 near $x = 0$ to 0.00088 near $x = \pm L$. Nevertheless, according to Figs. 11–13, the numerical results match very well with the exact solutions for all three cases. The only exception is that, for cases (ii) and (iii) where $r = 2$ and $r = 4$, respectively, there are small solution bumps near interfaces separating mesh intervals of vastly different sizes. It is interesting to note that solution accuracy at points away from these interfaces are not impacted by these bumps.

7.2 Propagation of Sound Waves through a Transonic Nozzle

The benchmark problem 1.1 in the third Computational Aeroacoustics (CAA) Workshop that have been solved using the 2D CE/SE Euler solver with adjustable numerical dissipation in [44] are used to test the 2D Euler version of scheme w-2 described above. The same 401 stretching mesh used in [44] is used here. As shown in Fig. 14, the current numerical results agree very well with the exact solutions.

7.3 Oblique shock reflection

The oblique shock reflection problem[7] is solved using 9600 (120x40x2) uniformly-distributed structured triangles with $\Delta t = 0.005$ and 0.0005, respectively. For $\Delta t = 0.005$, the Courant number is in the order of 1. Numerical results obtained using different models are very similar. However, for $\Delta t = 0.0005$, the solution obtained using an old CE/SE scheme becomes very dissipative. In contrast, as shown in Fig. 15, the numerical solutions obtained using the 2D Euler version of scheme w-2 still preserve sharp shock resolution.

8. Conclusions and discussions

Generally speaking, a stable numerical marching for a non-linear problem requires the presence of a sufficient amount of numerical dissipation. However, accuracy of the numerical results, especially for an unsteady problem, will suffer if too much numerical dissipation is present. As such, a careful con-

trol of numerical dissipation is a must for an accurate and stable non-linear unsteady numerical simulation. However, a proper control of numerical dissipation is a very difficult task. Although one can increase the numerical dissipation rather easily, it is much harder to reduce it when accuracy consideration requires it.

The CE/SE method is developed from a set of non-dissipative solvers. As such each CE/SE solver is an extension of a core non-dissipative scheme. *It is this unique feature that make it much easier to reduce numerical dissipation in a CE/SE simulation. It is also the key reason behind the successful construction of the Courant number insensitive CE/SE schemes described in this paper.*

In this paper, the ideas used in a recent work on one-dimensional CFL number insensitive schemes are elaborated in a much more detailed manner. These ideas are also extended to construct one-dimensional and multidimensional solvers for applications involving nonuniform meshes. The advantages of the new schemes over the original CE/SE schemes are overwhelming and clearly demonstrated by the numerical results presented.

In addition, we also report advances in developing new wiggle-suppressing techniques. These new techniques are based on a new set of weighted averaging formulae which are much more potent and flexible than those introduced earlier.

Finally note that, in addition to the Euler applications reported in this paper and [35,36], the CFL number insensitive schemes recently have also been applied to (i) Navier-Stokes problems by C.L. Chang [42]; and (ii) chromatographic adsorption problems [43] by Y.I. Lim *et al.*

References

1. S.C. Chang and W.M. To, *A New Numerical Framework for Solving Conservation Laws—The Method of Space-Time Conservation Element and Solution Element*, NASA TM 104495, August 1991.
2. S.C. Chang and W.M. To, A brief description of a new numerical framework for solving conservation laws—The method of space-time conservation element and solution element, in *Proceedings of the Thirteenth International Conference on Numerical Methods in Fluid Dynamics, Rome, Italy, 1992*, edited by M. Napolitano and F. Sabetta, Lecture Notes in Physics 414, (Springer-Verlag, New York/Berlin, 1992), p. 396.
3. S.C. Chang, The method of space-time conser-

- vation element and solution Element—A new approach for solving the Navier-Stokes and Euler equations, *J. Comput. Phys.*, **119**, 295 (1995).
4. S.C. Chang, S.T. Yu, A. Himansu, X.Y. Wang, C.Y. Chow, and C.Y. Loh, The method of space-time conservation element and solution element—A new paradigm for numerical solution of conservation laws, in *Computational Fluid Dynamics Review 1998* edited by M.M. Hafez and K. Oshima (World Scientific, Singapore), Vol. 1, p. 206.
 5. T. Molls and F. Molls, “Space-Time Conservation Method Applied to Saint Venant Equations,” *J. of Hydraulic Engr.*, **124(5)**, 501 (1998).
 6. C. Zoppou and S. Roberts, “Space-Time Conservation Method Applied to Saint Venant Equations: A Discussion,” *J. of Hydraulic Engr.*, **125(8)**, 891 (1999).
 7. S.C. Chang, X.Y. Wang, and C.Y. Chow, The space-time conservation element and solution element method: A new high-resolution and genuinely multidimensional paradigm for solving conservation laws,” *J. Comput. Phys.*, **156**, 89 (1999).
 8. X.Y. Wang, and S.C. Chang, A 2D non-splitting unstructured triangular mesh Euler solver based on the space-time conservation element and solution element method, *Computational Fluid Dynamics Journal*, **8(2)**, 309 (1999).
 9. S.C. Chang, X.Y. Wang and W.M. To, Application of the space-time conservation element and solution element method to one-dimensional convection-diffusion problems, *J. Comput. Phys.*, **165**, 189 (2000).
 10. J. Qin, S.T. Yu, Z.C. Zhang, and M.C. Lai, Direct Calculations of Cavitating Flows by the Space-Time CE/SE Method, *J. Fuels & Lubricants*, *SAE Transc.*, **108(4)**, 1720 (2000).
 11. C.Y. Loh, L.S. Hultgren and S.C. Chang, Wave computation in compressible flow using the space-time conservation element and solution element method, *AIAA J.*, **39(5)**, 794 (2001).
 12. Z.C. Zhang, S.T. Yu, and S.C. Chang, A Space-Time Conservation Element and Solution Element Method for Solving the Two- and Three-Dimensional Unsteady Euler Equations Using Quadrilateral and Hexahedral Meshes, *J. Comput. Phys.*, **175**, 168 (2002).
 13. K.B.M.Q. Zaman, M.D. Dahl, T.J. Bencic, and C.Y. Loh, Investigation of A ‘Transonic Resonance’ with Convergent-Divergent Nozzles, *J. Fluid Mech.*, **463**, 313 (2002).
 14. C.Y. Loh and K.B.M.Q. Zaman, *Numerical Investigation of ‘Transonic Resonance’ with A Convergent-Divergent Nozzle*, *AIAA J.*, **40(12)**, 2393 (2002).
 15. X.Y. Wang, C.Y. Chow, and S.C. Chang, *Numerical Simulation of Flows Caused by Shock-Body Interaction*, AIAA Paper 96-2004 (1996).
 16. S.C. Chang, A. Himansu, C.Y. Loh, X.Y., Wang, S.T., Yu, and P. Jorgenson, Robust and Simple Non-Reflecting Boundary Conditions for the Space-Time Conservation Element and Solution Element Method, in *A Collection of Technical Papers, 13th AIAA CFD Conference, June 29-July 2, 1997, Snowmass, Colorado*, AIAA Paper 97-2077.
 17. C.Y. Loh, L.S. Hultgren and S.C. Chang, *Vortex Dynamics Simulation in Aeroacoustics by the Space-Time Conservation Element and Solution Element Method*, AIAA Paper 99-0359 (1999).
 18. X.Y. Wang, S.C. Chang and P.C.E. Jorgenson, *Accuracy Study of the Space-Time CE/SE Method for Computational Aeroacoustics Problems Involving Shock Waves*, AIAA Paper 2000-0474 (2000).
 19. C.Y. Loh, L.S. Hultgren, S.C. Chang and P.C.E. Jorgenson, *Noise Computation of a Supersonic Shock-Containing Axisymmetric Jet by the CE/SE Method*, AIAA Paper 2000-0475 (2000).
 20. C.Y. Loh, X.Y. Wang, S.C. Chang, and P.C.E. Jorgenson, Computation of Feedback Aeroacoustic System by the CE/SE Method, in *Proceedings of the First International Conference on Computational Fluid Dynamics, Kyoto, Japan, 10-14 July, 2000*, edited by N. Sato-fuka, (Springer-Verlag Berlin Heidelberg 2001), p. 555.
 21. C.Y. Loh, L.S. Hultgren and P.C.E. Jorgenson, *Near Field Screech Noise Computation for An Underexpanded Supersonic Jet by the CE/SE Method*, AIAA Paper 2001-2252 (2001).

22. X.Y. Wang, S.C. Chang, and P.C.E. Jorgenson, Numerical Simulation of Aeroacoustic Field in a 2D Cascade Involving a Downstream Moving Grid Using the Space-Time CE/SE method, in *Proceedings of the First International Conference on Computational Fluid Dynamics, Kyoto, Japan, 10-14 July, 2000*, edited by N. Satofuka, (Springer-Verlag Berlin Heidelberg 2001), p. 543.
23. X.Y. Wang, S.C. Chang, A. Himansu, and P.C.E. Jorgenson, *Gust Acoustic Response of A Single Airfoil Using the Space-Time CE/SE Method*, AIAA Paper 2002-0801 (2002).
24. S.T. Yu and S.C. Chang, *Treatments of Stiff Source Terms in Conservation Laws by the Method of Space-Time Conservation Element and Solution Element*, AIAA Paper 97-0435 (1997).
25. S.T. Yu and S.C. Chang, Applications of the Space-Time Conservation Element / Solution Element Method to Unsteady Chemically Reactive Flows,” AIAA Paper 97-2099, in *A Collection of Technical Papers, 13th AIAA CFD Conference*, June 29-July 2, 1997, Snowmass, CO.
26. S.T. Yu, S.C. Chang, P.C.E. Jorgenson, S.J. Park and M.C. Lai, “Treating Stiff Source Terms in Conservation Laws by the Space-Time Conservation Element and Solution Element Method,” in *Proceedings of the 16th International Conference on Numerical Method in Fluid Dynamics, Arcachon, France, 6-10 July, 1998*, edited by C.H. Bruneau, (Springer-Verlag Berlin Heidelberg 1998), p. 433.
27. X.Y. Wang and S.C. Chang, A 3D structured/unstructured Euler solver based on the space-time conservation element and solution element method, in *A Collection of Technical Papers, 14th AIAA CFD Conference, June 28-July 1, 1999, Norfolk, Virginia*, AIAA Paper 99-3278.
28. N.S. Liu and K.H. Chen, *Flux: An Alternative Flow Solver for the National Combustion Code*, AIAA Paper 99-1079.
29. G. Cook, *High Accuracy Capture of Curved Shock Front Using the Method of Conservation Element and Solution Element*, AIAA Paper 99-1008.
30. S.C. Chang, Y. Wu, X.Y. Wang, and V. Yang, Local Mesh Refinement in the Space-Time CE/SE Method, in *Proceedings of the First International Conference on Computational Fluid Dynamics, Kyoto, Japan, 10-14 July, 2000*, edited by N. Satofuka, (Springer-Verlag Berlin Heidelberg 2001), p. 61.
31. S.C. Chang, Z.C. Zhang, S.T. John Yu, and P.C.E. Jorgenson, A Unified Wall Boundary Treatment for Viscous and Inviscid Flows in the CE/SE Method, in *Proceedings of the First International Conference on Computational Fluid Dynamics, Kyoto, Japan, 10-14 July, 2000*, edited by N. Satofuka, (Springer-Verlag Berlin Heidelberg 2001), p. 671.
32. Z.C. Zhang, S.T. John Yu, S.C. Chang, and P.C.E. Jorgenson, Calculations of Low-Mach-Number Viscous Flows without Preconditioning by the Space-Time CE/SE method, in *Proceedings of the First International Conference on Computational Fluid Dynamics, Kyoto, Japan, 10-14 July, 2000*, edited by N. Satofuka, (Springer-Verlag Berlin Heidelberg 2001), p. 127.
33. A. Himansu, P.C.E. Jorgenson, X.Y. Wang, and S.C. Chang, Parallel CE/SE Computational via Domain Decomposition, in *Proceedings of the First International Conference on Computational Fluid Dynamics, Kyoto, Japan, 10-14 July, 2000*, edited by N. Satofuka, (Springer-Verlag Berlin Heidelberg 2001), p. 423.
34. Y. Wu, V. Yang, and S.C. Chang, Space-Time Method for Chemically Reacting Flows with Detailed Kinetics, in *Proceedings of the First International Conference on Computational Fluid Dynamics, Kyoto, Japan, 10-14 July, 2000*, edited by N. Satofuka, (Springer-Verlag Berlin Heidelberg 2001), p. 207.
35. S.C. Chang, *Courant Number Insensitive CE/SE Schemes*, AIAA Paper 2002-3890 (2002).
36. M. Zhang, S.T. Yu, and S.C. Chang, *CFL Number Insensitive CESE Schemes For Two-Dimensional Euler Equations*, AIAA Paper 2003-3840 (2003).
37. Other CE/SE references are posted on: <http://www.grc.nasa.gov/www/microbus>.
38. B. van Leer, Toward the Ultimate Conservative Difference Scheme. IV. A New Approach to Numerical Convection, *J. Comput. Phys.*, **23**, 276 (1977).

39. G.D. van Albada, B. van Leer, and W.W. Robert, A Comparative Study of Computational Methods in Cosmic Gas Dynamics, *Astronom. and Astrophys.*, **108**, 76 (1982).
40. To appear in a NASA Technical Memorandum.
41. G.A. Sod, A Survey of several Finite Difference Methods for Systems of Nonlinear Hyperbolic Conservation Laws, *J. Comput. Phys.*, **27**, 1 (1978).
42. Chau-Lyan Chang, private communication.
43. Y.I. Lim, S.C. Chang, and S.B. Jorgensen, A Novel Partial Differential Algebraic Equation (PDAE) Solver: Iterative Space-Time Conservation Element/Solution Element (CE/SE) Method, submitted for publication in *Comp. Chem. Eng.*.
44. X.Y. Wang, S.C. Chang, and P.C.E. Jorgenson, *Prediction of Sound Waves Propagating through a Nozzle without/with a Shock Wave Using the Space-time CE/SE Method*, AIAA Paper 2000-0222 (2000).

Table I. The values of function $f(K = 3, M = 4)$

k	0	0	0	0	1	1	1	1	2	2	2	2	3
m	0	1	2	3	0	1	2	3	0	1	2	3	0
$f(k, m)$	0	$\frac{1}{2}$	1	$\frac{3}{2}$	2	$\frac{5}{2}$	3	$\frac{7}{2}$	4	$\frac{9}{2}$	5	$\frac{11}{2}$	6

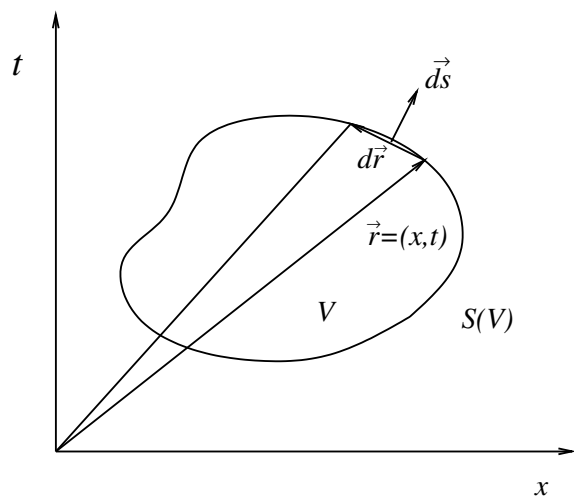
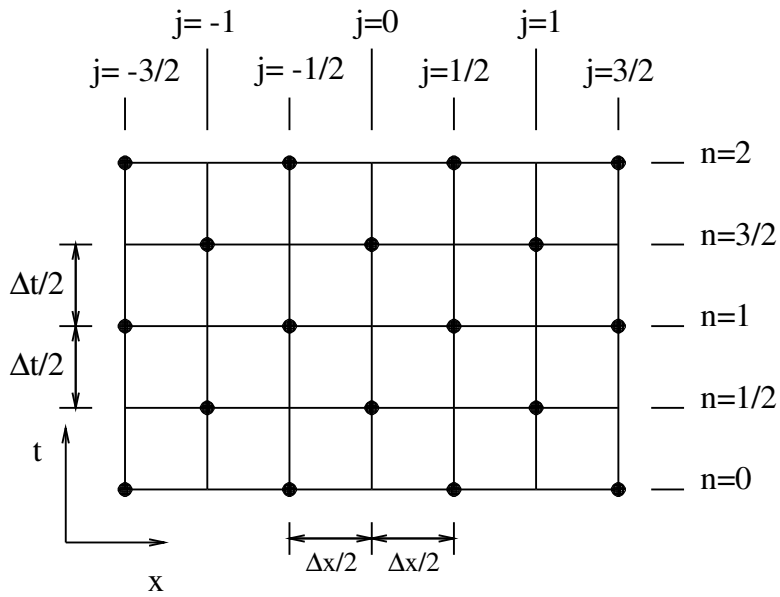
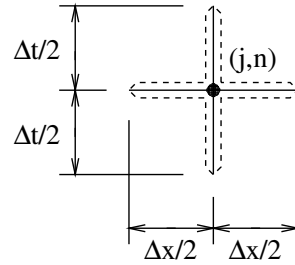


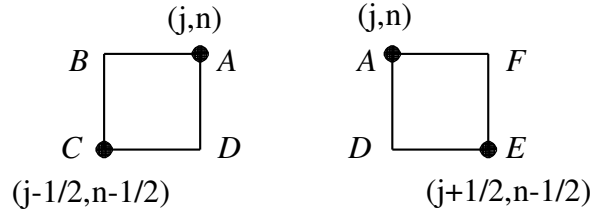
Figure 1. — A surface element on the boundary $S(V)$ of an arbitrary space-time volume V .



2(a). — The space-time mesh.

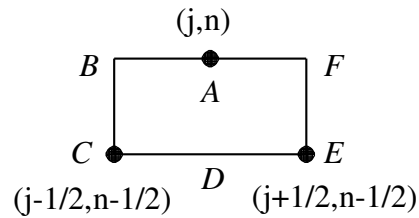


2(b). — SE(j,n)



2(c). CE₋(j,n)

2(d). CE₊(j,n)



2(e). CE(j,n)

Figure 2. — The SEs and CEs.

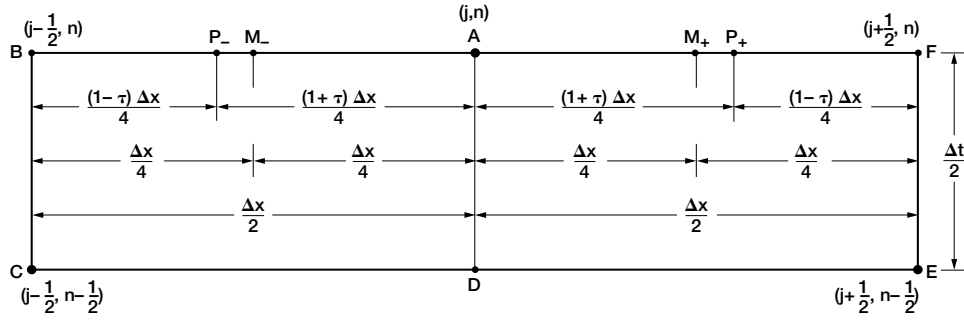


Figure 3.—Definition of points P_- , M_- , M_+ , and P_+ .

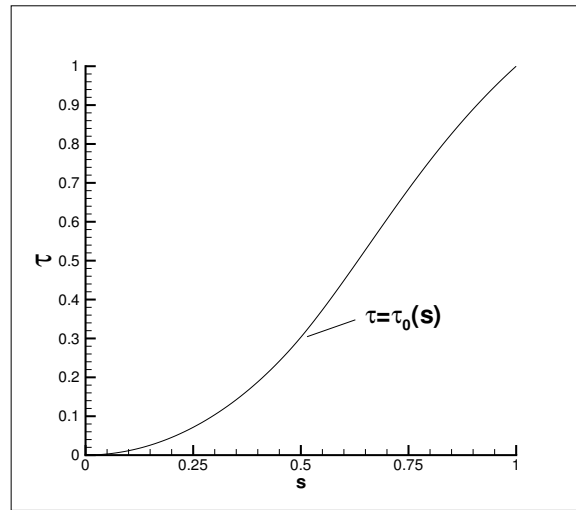


Figure 4. The function $\tau_0(s)$.

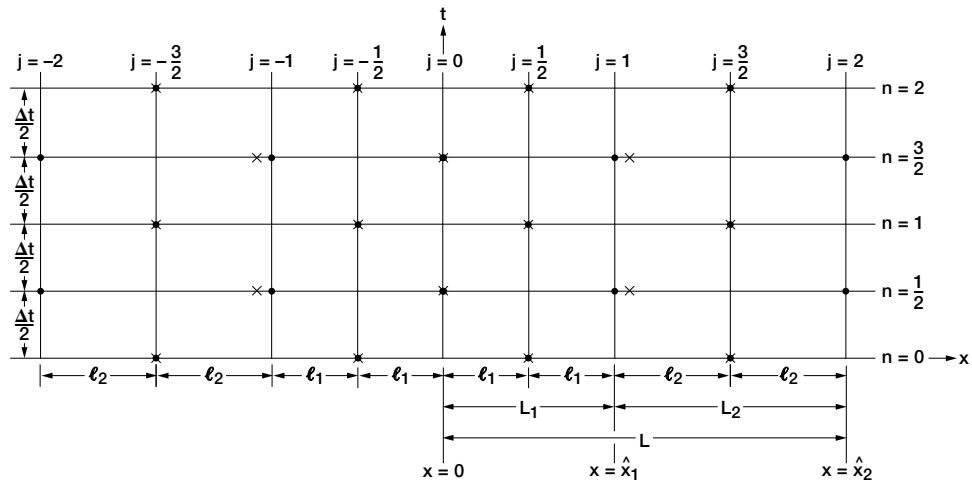


Figure 5.—A space-time mesh with nonuniform spatial intervals ($K = M = 2$).

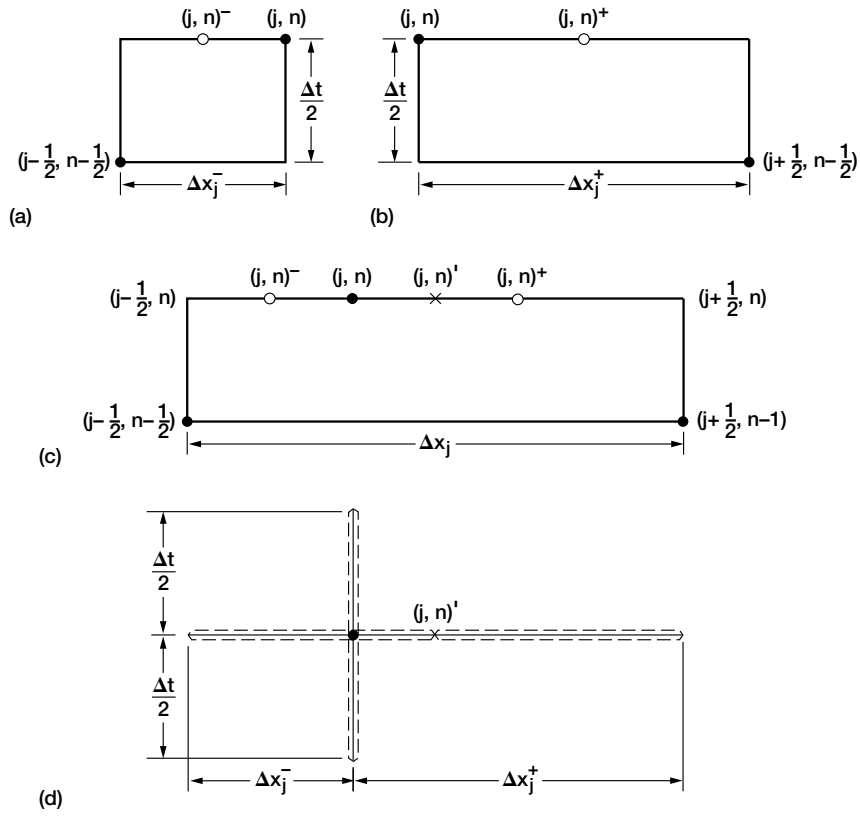


Figure 6.—The SEs and CE for a nonuniform mesh. (a) $CE_{-}(j,n)$. (b) $CE_{+}(j,n)$. (c) $CE(j,n)$. (d) $SE(j,n)$.

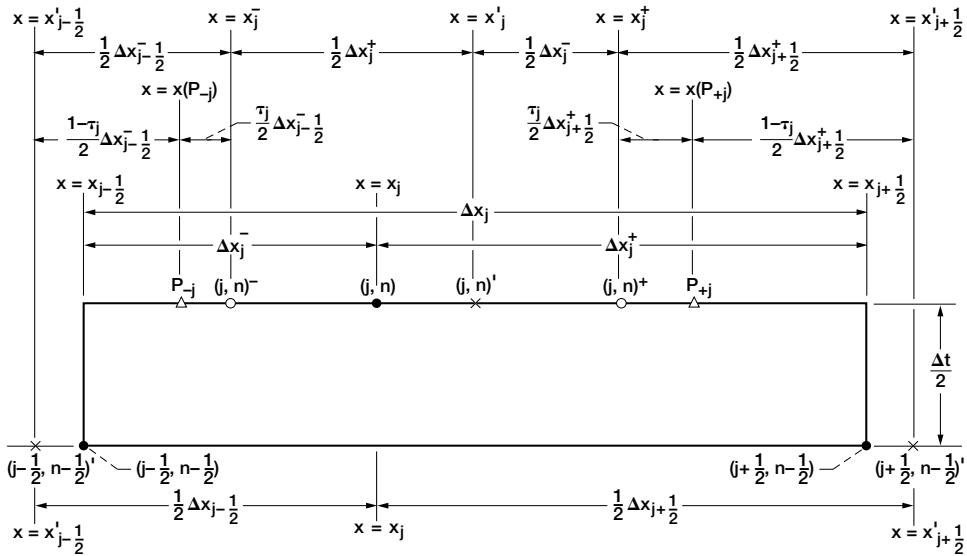


Figure 7.—Key geometric parameters and their relations.

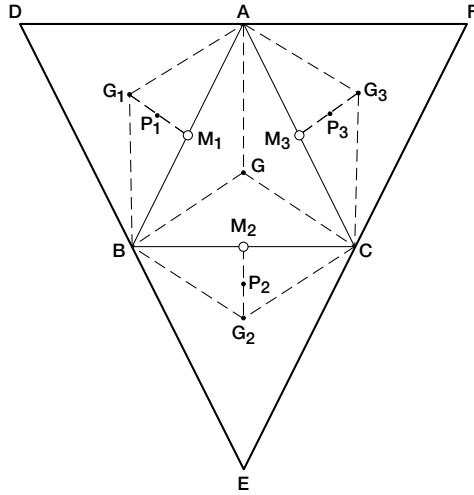


Figure 8.—Definition of points $P_1, P_2, P_3, M_1, M_2,$ and M_3 .

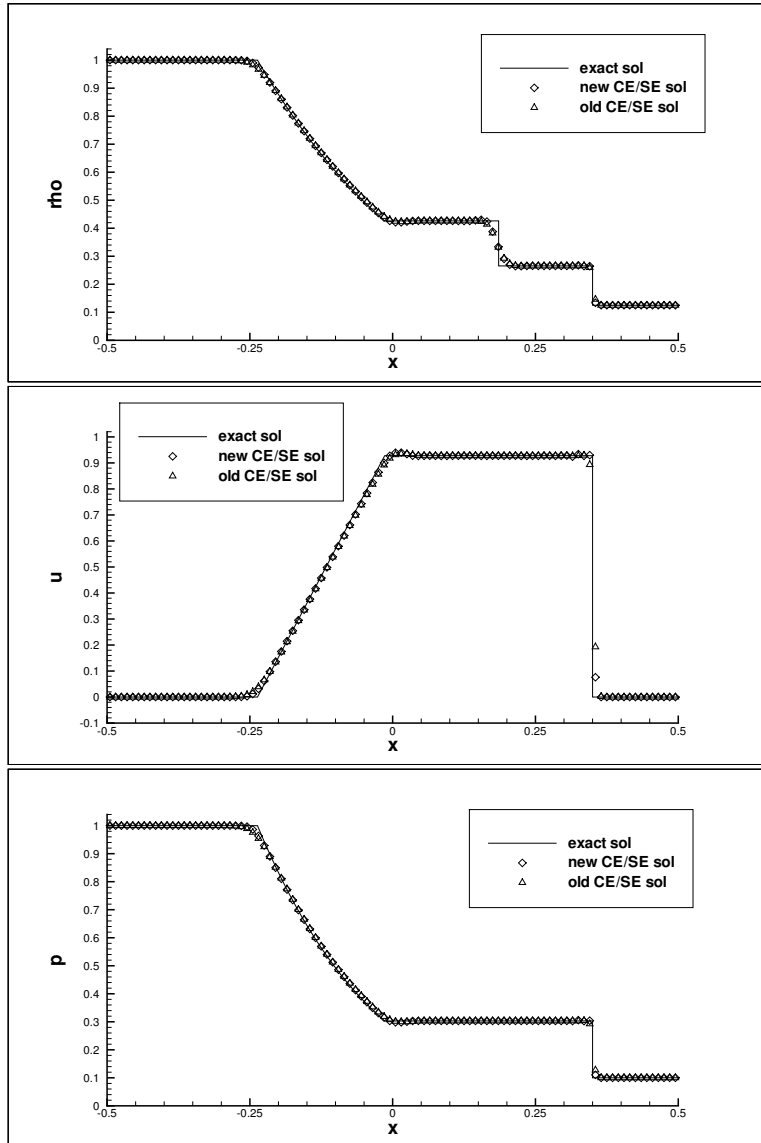


Figure 9: Uniform-mesh solutions to Sod's problem (CFL number = 0.88).

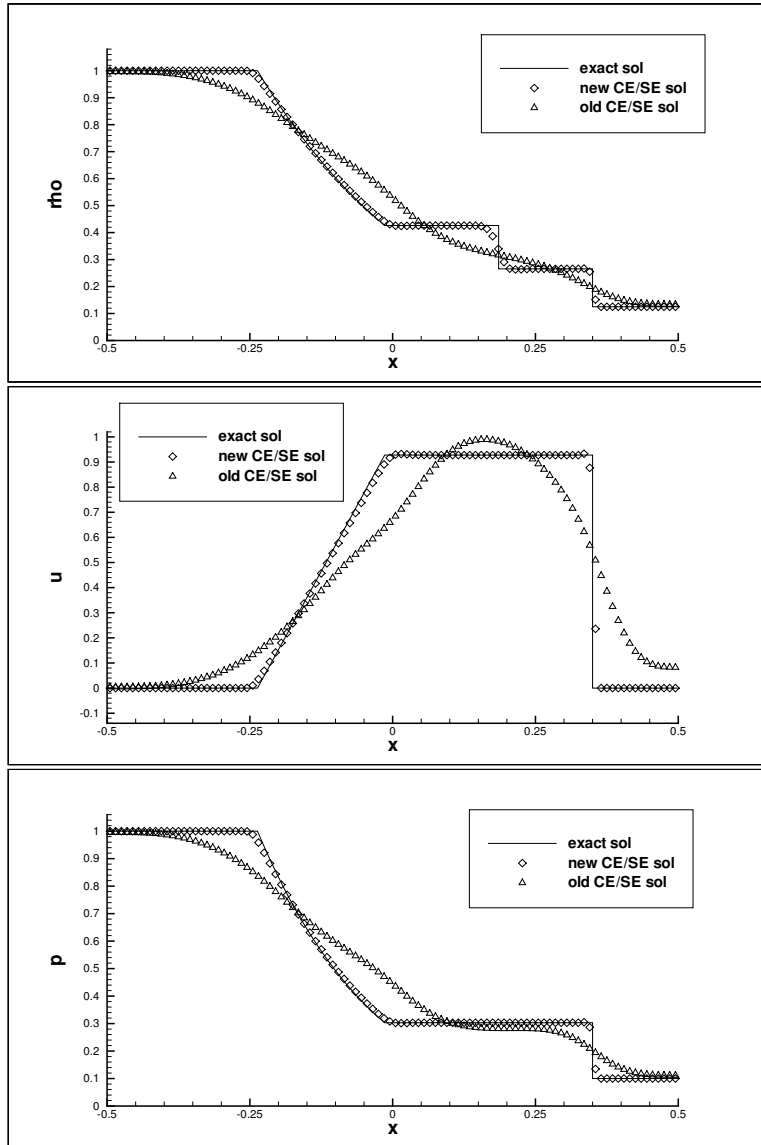


Figure 10: Uniform-mesh solutions to Sod's problem (CFL number = 0.00088).

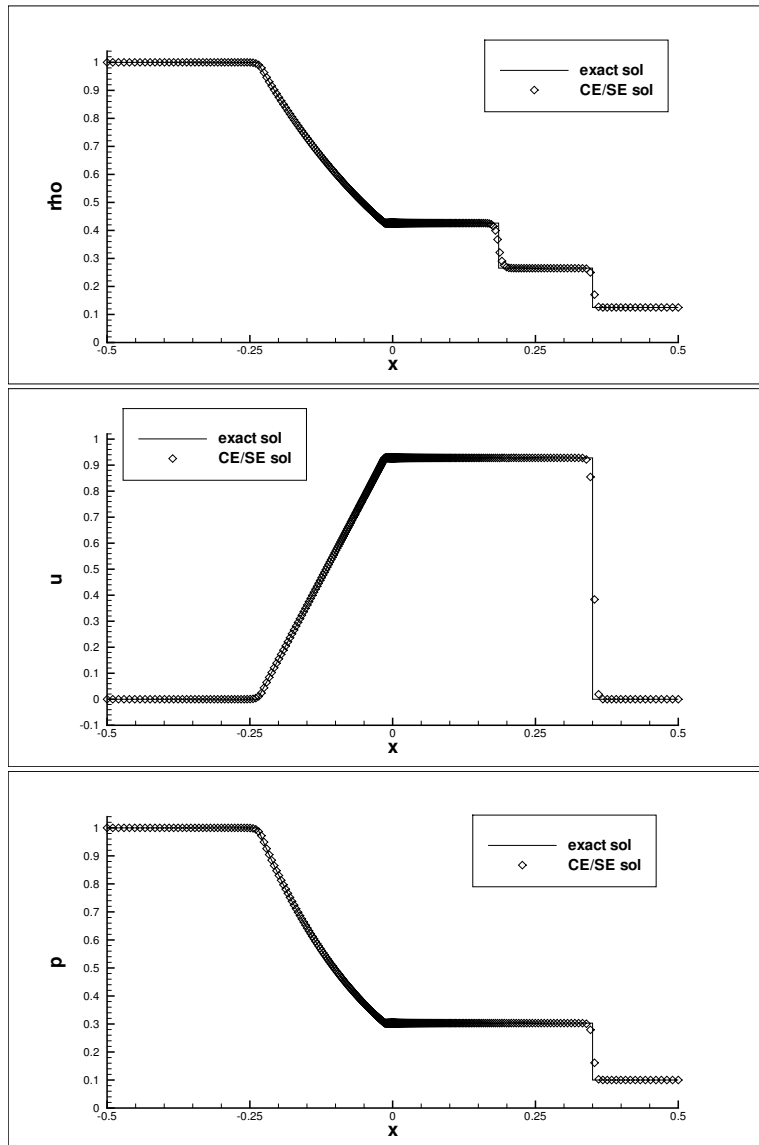


Figure 11: Nonuniform-mesh solutions to Sod's problem ($L = 0.5$, $r = 1/0.96$, $M = 4$, $K = 170$).

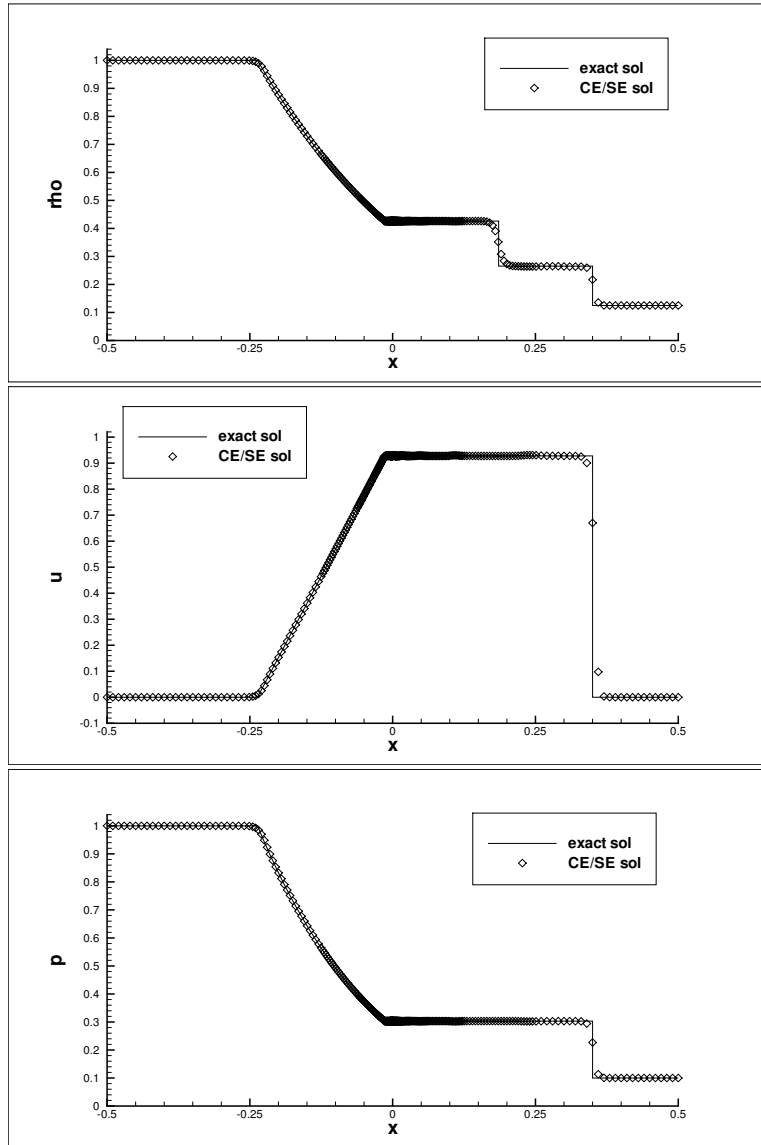


Figure 12: Nonuniform-mesh solutions to Sod's problem ($L = 0.5, r = 2, M = 50, K = 11$).

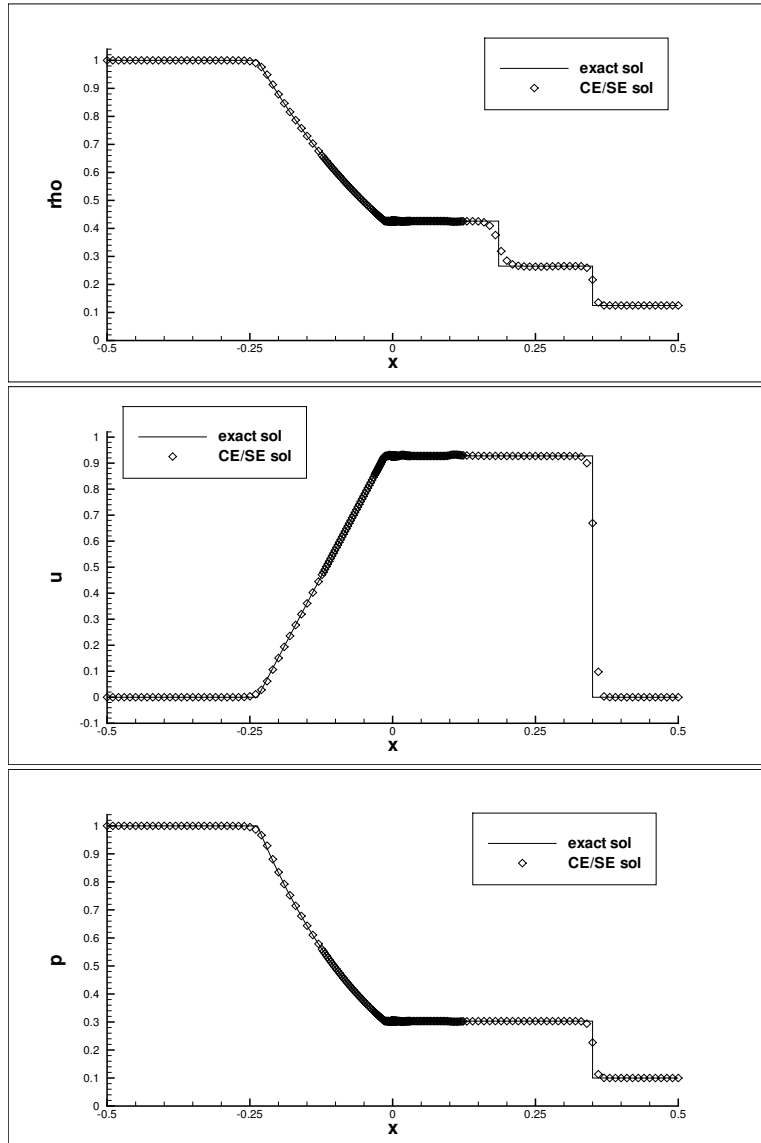


Figure 13: Nonuniform-mesh solutions to Sod's problem ($L = 0.5, r = 4, M = 75, K = 6$).

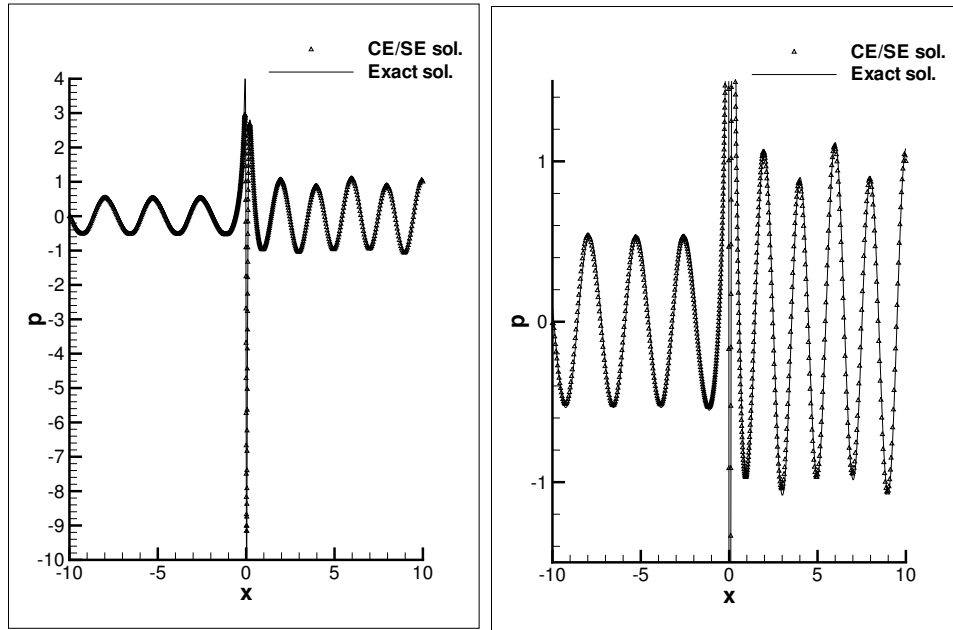


Figure 14: CE/SE solution of the acoustic wave using a 401 point nonuniform mesh.

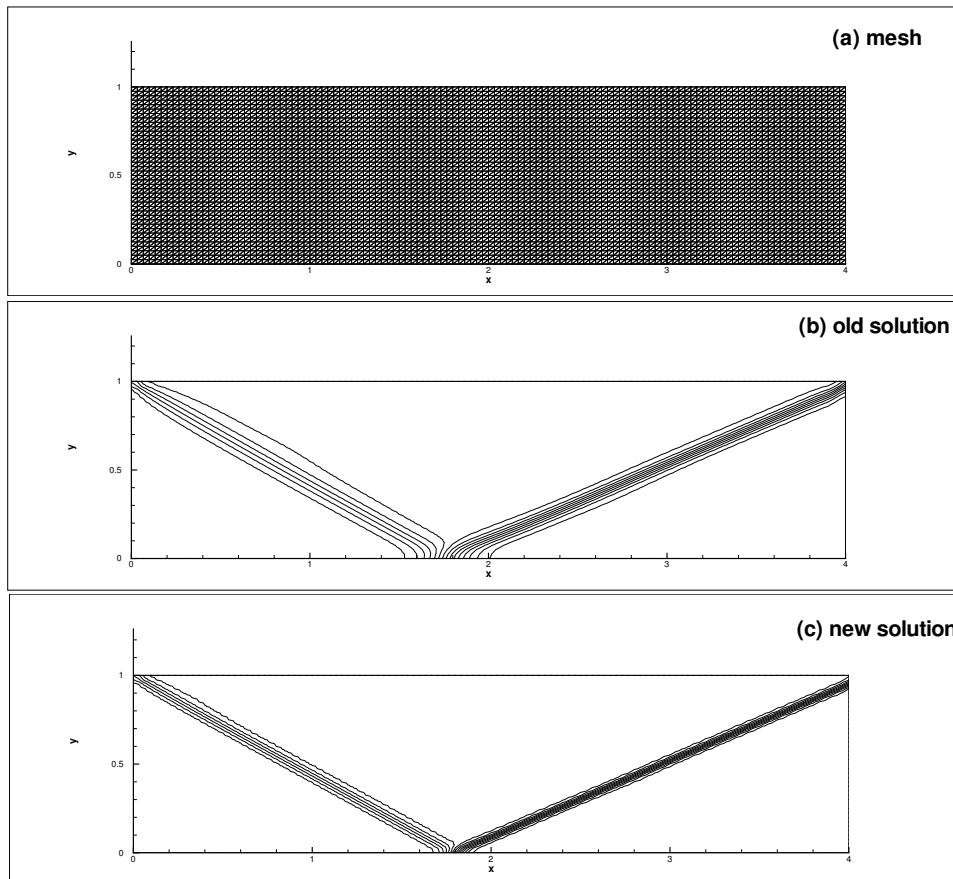


Figure 15: CE/SE solution of the oblique shock problem on a uniform mesh with $\Delta t = 0.0005$.